THE DEVELOPMENT OF A PULSED PLASMA LABORATORY FOR STUDYING THE THERMOPHYSICAL PROPERTIES OF HIGH PRESSURE PLASMA

A THESIS

Presented to

The Faculty of the Division

of Graduate Studies

By

Peter C. Brookes

In Partial Fulfillment

of the Requirements for the Degree

Master of Science in the School

of Mechanical Engineering

Georgia Institute of Technology

December, 1977

THE DEVELOPMENT OF A PULSED PLASMA LABORATORY FOR STUDYING THE THERMOPHYSICAL PROPERTIES OF HIGH PRESSURE PLASMA

Approved:

A. V. Larson, Chairman

T. W. Jackson

J. M. Mills

Date approved by Chairman: 12/5/77

ACKNOWLEDGMENTS

I wish to thank Dr. A. V. Larson for providing this opportunity and the sound advice and guidance without which this thesis could not have been written; Mr. T. E. Clopton for so freely giving his time and electronics expertise; and especially Mr. R. T. Murray for sharing his knowledge and experience, for patiently teaching research techniques, and for his sincere interest in my development.

TABLE OF CONTENTS

LIST OF TABLES

LIST OF ILLUSTRATIONS

NOMENCLATURE

Symbols

A	charge integration constant
A	cross-sectional area
B	current integration constant
B_m	magnetic field intensity
b	number of circuit branches
C	capacitance
D	rate of current change integration constant
d	diameter
E	energy
EMF	electromotive force
f	focal length
f	mole fraction
H	enthalpy
I	radiant intensity
i	current
i	image distance
j	imaginary units
K	Boltzmann's constant
L	inductance
ℓ	circumference
l	length
M	molecular weight

N_{AV}	Avogadro's number
N	particle number
N	number of windings
n	winding density
O	object distance
P	power
P	pressure
q	charge
R	resistance
R_C	major radius
r	radius
T	temperature
T	period
t	time
V	voltage
V	volume
X	reactance
Z	impedance

Units

A	amperes
atm	atmospheres
C	centigrade
cm	centimeter
eV	electron volt
g	gram
Hz	Hertz

J	Joule
K	Kelvin
KA	kiloampere
KV	kilovolt
m	meter
mA	milliamp
mm	millimeter
MΩ	megohm
ns	nanosecond
Nt	Newton
rad	radian
s	second
V	volt
W	Watt
Ω	ohm
μA	microampere
μF	microfarad
μH	microhenry
μm	micrometer
μs	microsecond

SUMMARY

A Pulsed Plasma Facility enables the production of plasma from ambient gas on a microsecond timescale. Temperatures around 10^4°K and pressures exceeding 100 atm are easily achieved. The plasma is created via an electrical discharge across a confined gap by a high energy and voltage capacitor bank. By adjusting the power level, the thermophysical properties of plasma at varying pressures can be determined.

The development of the laboratory concerned:

(1) Designing a discharge cell suitable for spectroscopic analysis.

(2) Shaping the discharge current to obtain favorable plasma conditions.

(3) Devising a method for preionizing the cell to initiate the discharge.

(4) Developing instrumentation for monitoring the plasma spectroscopically and electrically, and for control of failure modes.

CHAPTER I

INTRODUCTION

A plasma is basically an aggregation of electrons and ions--the latter being singly or multiply charged, atomic or molecular in nature. If a sufficient quantity of energy is imparted to a gas via electrical discharge, it becomes a plasma. The increase in kinetic energy of the gas particles results in intense collisions which dissociate electrons from atoms and molecules and even break the bonds of the latter. Plasma is electrically neutral on average due to the inherent balance of positive and negative charges. Its quasineutrality and collective behavior due to long range coulombic forces distinguish plasma from gas, which itself is partially ionized even in the ambient condition. In fact, plasma has been termed the "fourth state of matter."

Similar to solids, liquids, and gases, matter as a plasma exhibits thermophysical properties different from the same properties in another state. Within the plasma domain itself, properties likewise depend upon the thermodynamic variables defining the state. The objective of plasma diagnostics is to determine the thermophysical properties as functions of pressure, temperature, and mole fraction.

Increasing the internal energy of gas upon the

transition to plasma is not the exclusive result of energy deposition. The loss mechanisms of heat transfer are important at plasma temperatures. Radiation is the principle mode especially at high pressures. Line and continuum radiation are emitted by the excited particles and their spectroscopic analysis reveals many plasma properties.

Two basic electric arc methods exist for creating a plasma suitable for investigation, although several variants exist for applying them. These are the steady-state arc, whereby the plasma exists in equilibrium for relatively long durations, and the pulsed arc, in which a temporary plasma is created via a capacitive discharge. The former technique is currently employed in the Mechanical Engineering High Pressure Laboratory using the Maecker cascade shown schematically in Figure I-1. The cascade forms a stable arc by constraining it to a circular channel in the center of a stack of copper water-cooled plates which are electrically insulated from one another and maintained at different floating potentials by the discharge. Gas at the desired pressure is introduced into the channel via injection ports and the plasma formed between the two electrodes is spectroscopically diagnosed through the central observation port. Due to corrosion by such gases as air at high temperatures, the electrodes are shielded by inert argon gas.

The Pulsed Plasma Facility basically employs a high power capacitive discharge across an interelectrode gap

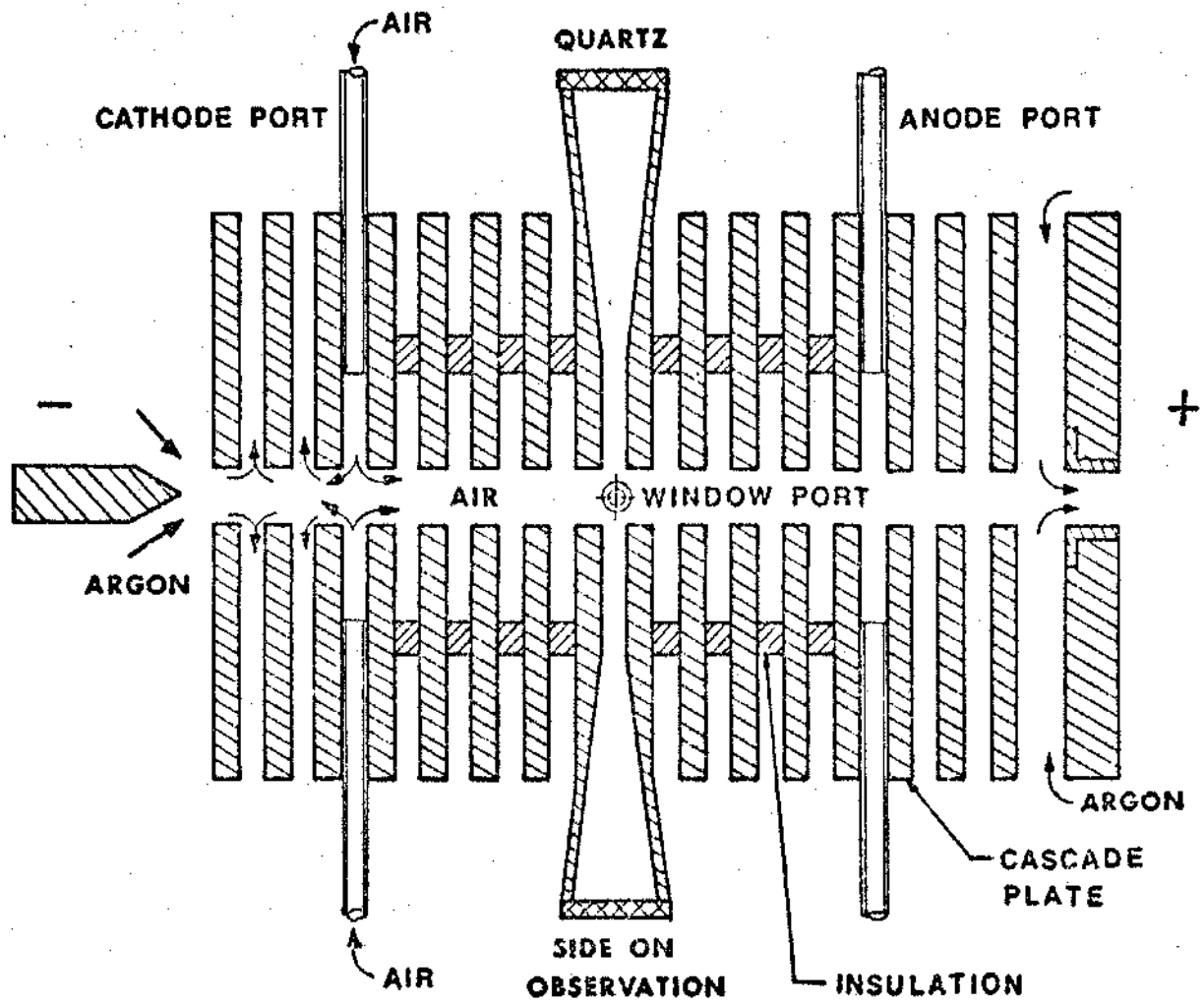

Figure I-1. Schematic Diagram of Steady-State Arc Apparatus

inside a confinement vessel filled with gas. By adjusting the electrical power input, plasma of the desired pressure can be obtained starting from the ambient state. The time-varying pressure and temperature require diagnostic methods differing from those employed in studying the cascade arc. The details of these and other facets of laboratory development and design constitute this thesis and are presented later.

Although both are valuable diagnostic techniques, the pulsed method possesses certain advantages:

(1) External arc stabilization is not required due to the temporary nature of the discharge.

(2) The arc operates at very high peak power but low average power--enabling usage of low average power devices.

(3) Wall cooling is not required due to the low average power.

(4) Chemistry problems are less severe or absent.

(5) Certain radiation transport problems between the plasma and the detector are reduced.

The Pulsed Plasma Facility should be a valuable addition to the existing laboratory. The principle objectives which instigated its development are:

(1) To provide independent experimental confirmation of the results of the steady-state research.

(2) To acquire data at pressures and power levels not yet attempted in the steady-state facility. New

experimental information is thus produced and problems in diagnostics of high pressure plasma can be discovered--helping to form guidelines for similar steady-state research.

Presented in the following pages is a detailed description of the laboratory--its design and governing theories, its components, the necessary experiments and calibrations, and the information available from the facility. Any suitable gas can be used for plasma production, but air shall be employed in the initial study and is therefore referenced in several design calculations.

CHAPTER II

CELL DESIGN

The heart of the set-up is the discharge cell in which gas becomes a plasma at pressures reaching several hundred atmospheres. A capacitive discharge across an open gap produces a radially expanding plasma which develops only dynamic pressure due to the infinite volume available. By confining the plasma by enclosing walls to the interelectrode gap however, high instantaneous pressures can be generated.

The discharge cell must meet the following design requirements:

(1) It must define a volume capable of creating the desired plasma state.

(2) It must withstand high pressures.

(3) It must be optically transparent in the near infrared through ultraviolet wavelength ranges.

(4) It must maintain a constant volume and geometry.

(5) It must allow only minimal leakage at high internal pressure.

(6) It must be capable of repeated experiments at varying energy input levels.

(7) It must permit spectroscopic analysis and back-lighting of the plasma.

(8) It should present minimal analysis problems concerning the radiation optics.

(9) It must minimize the possibility of high voltage arcover outside the plasma volume.

(10) It must allow minimal plasma contamination during the discharge.

The cell designed to meet this criteria is shown in Figure II-1. It stems conceptually from the work of S. N. Andreev and T. V. Gavrilova of the Soviet Union [1] although several modifications have been implemented to improve its usefulness. While designed to study any gas, air is employed in the initial experiment.

The plasma volume is 1.1 x 1.0 x 10 mm^3--the length being 10 mm and the cross-sectional area 1.1 mm^2. It is dimunitive because a large volume results in little pressure rise, while a small one of this geometry gives the desired static pressure rise with no dynamic pressure at the moment of maximum temperature. A quasi-steady-state analysis is thus possible. The chosen cross-section allows determination of the temperature and density distributions in a thin layer of plasma near the wall--spectroscopically advantageous for an optically thick high pressure plasma. The relatively long arclength permits viewing the central portion of the plasma away from the electrodes, which conduct heat from the cell and cool the bordering plasma.

The thermal properties and forces of the plasma

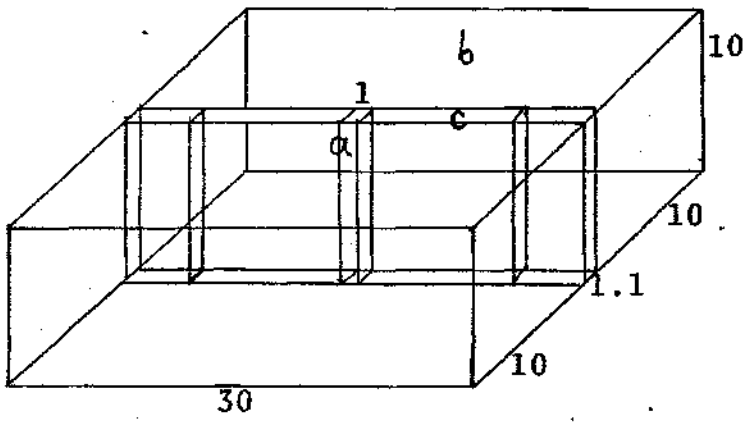

a = Plasma Volume
b = Quartz Plate
c = Quartz Gasket

Figure II-1A. Basic Plasma Volume of Cell

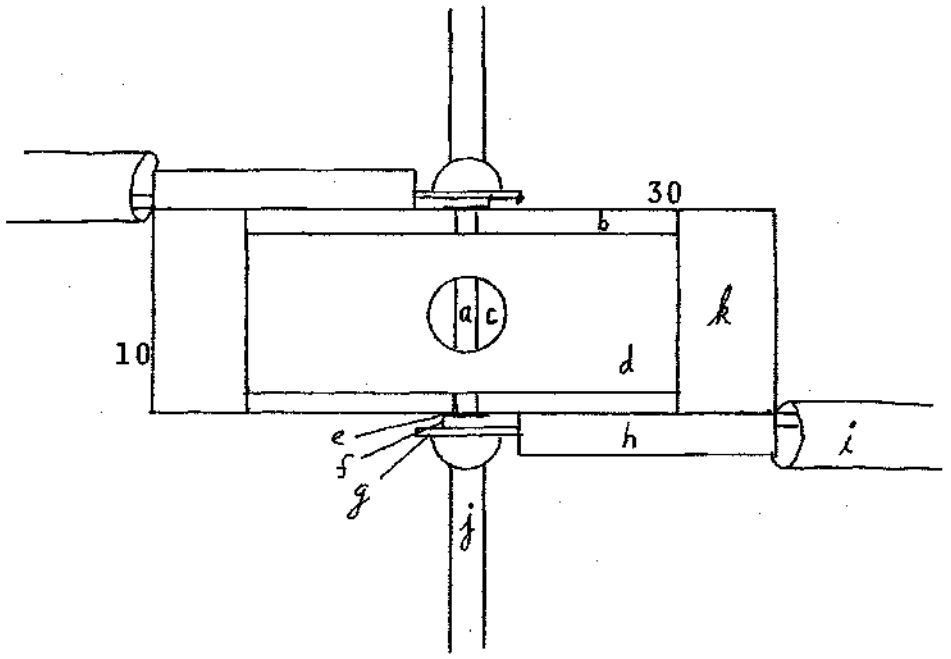

a = Plasma Volume
b = Quartz Plate
c = Viewing Port
d = Aluminum Plate
e = Platinum Electrode
f = Copper Lead
g = Teflon Sheet
h = Teflon Sheet
i = Teflon Tubing
j = Sheet Metal Clamp
k = Parallel Clamp

Figure II-1B. Side View of Complete Cell

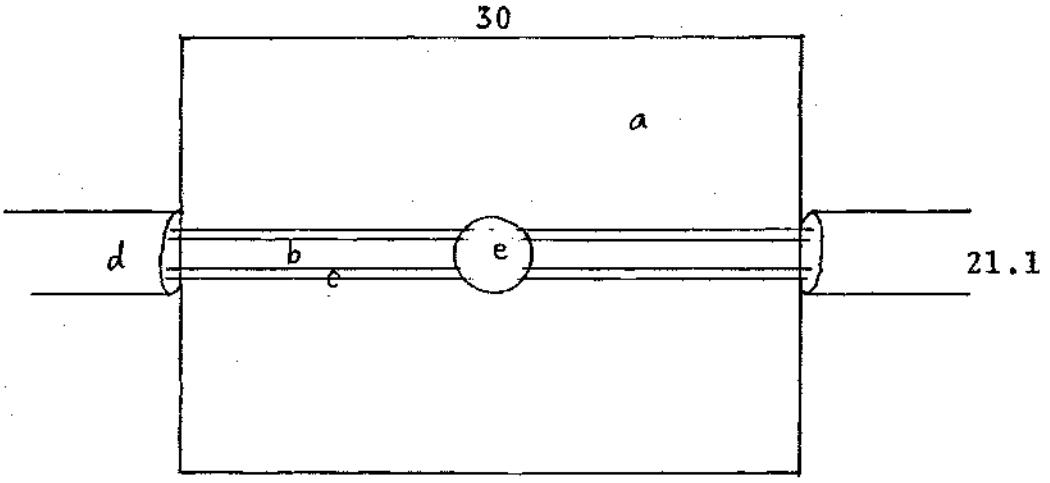

a = Quartz Plate
b = Copper Lead
c = Teflon Sheet
d = Teflon Tubing
e = Sheet Metal Clamp

Figure II-1C. Top View of Complete Cell

determine the choice of confinement material. The average temperature is calculated using the ideal gas law with a correction factor to account for departures from ideal-gas behavior:

$$T = \frac{P}{ZR\rho}$$

where

P = pressure

T = temperature

ρ = density

R = gas constant

Z = compressibility factor

Judging from previous experiments [4], the compressibility Z is around 1.3 for the desired state. The air density ρ is assumed constant at the ambient value of 1.2×10^{-3} g/cm^3 [1]. The pressure ranges over hundreds of atmospheres, and 100 atm is chosen for design purposes. With the gas constant for air being 2.83 cm^3-atm/g°K, the corresponding temperature is 2.27×10^4°K. 10^4°K is then the expected magnitude for the plasma temperature.

The force the plasma exerts on its confinement vessel at 100 atm (10^7 Nt/m^2) pressure is considerable. Its rectangular cross-section presents lateral surface areas of 10 mm^2 and 11 mm^2, with corresponding forces of 101.3 Nt

(22.8 lb_f) and 111.43 Nt (25.0 lb_f) according to the equation $F = PA$.

Suprasil quartz is chosen to constitute the containment vessel due to its desirable optical, thermal, electrical, and mechanical properties:

Transmission range	.2-1.1 μm
Transmittance	90%
Thermal conductivity	1.4 W/m°K
Dielectric strength	8 Kv/mm
Compression strength	$>1.1 \times 10^9$ Nt/m^2
Tensile strength	4.8×10^7 Nt/m^2
Rigidity modulus	3.1×10^{10} Nt/m^2

Quartz is extensively used for high temperature laboratory apparatus, being rather insensible to that property. It is electrically insulative and transparent to the radiation wavelength range to be studied. Its compression tolerance is 100 times and its rigidity 1000 times the forces to be encountered at 100 atm pressure.

The confining walls are thus constructed of two $10 \times 10 \times 30$ mm^3 plates and two $1.1 \times 10 \times 10$ mm^3 gaskets made of suprasil quartz smoothed to an optical flatness of their surfaces to insure good contact. They are fitted together as shown in Figure II-1 to surround the plasma volume with at least 10 mm of quartz to withstand the pressures generated.

Each electrode is a $4.6 \times 4.6 \times 0.2$ mm^3 sheet of

platinum alloy silver soldered (although spot welding is equally acceptable) to one end of a 3.2 x 0.9 x 38.1 mm^3 copper lead which extends lengthwise from the electrode to the edge of the cell. Platinum is the chosen electrode material because previous experients have shown that it contributes no emission lines to pulsed plasma radiation of proper discharge time [1].

The walls and electrodes are compressed and held stationary by parallel clamps and a sheet metal clamp, respectively. They eliminate the torquing characteristic of C-clamps. Due to the optical flatness of the quartz, sufficient compressional force will insure minimal air leakage without resorting to sealants which could contaminate the plasma. Aluminum plates, 8 x 10 x 1.6 mm^3, are placed on the quartz walls to distribute the compressional force and thereby lessen the possibility of local fracture. A circular viewing port 4 mm in diameter is drilled in each plate to allow spectroscopic analysis and backlighting of the plasma's central region. The ports are countersunk to lessen reflection problems.

Arcover between the electrodes to form the plasma requires attainment of breakdown voltage, which depends on the separation distance and the dielectric strength of the medium. The distance here is 10 mm and the dielectric strength of air is tabulated as 800 V/mm--thus requiring 8000 V across the gap for firing.

Due to the proximity of the clamps and copper leads, arcover outside the plasma chamber is possible at this voltage. Safeguards are implemented to prevent such lead-lead or lead-clamp discharges. The former employs the opposing lead entry scheme shown in Figure II-1 while the latter's breakdown voltage is increased by inserting a strong dielectric between them. Each copper lead is tightly surrounded by a .5 mm thick teflon sheet, whose dielectric strength is 60 KV/mm. A teflon sheet between the electrode and sheet metal clamp likewise protects them. The aluminum plates are naturally shielded by the quartz walls, whose dielectric strength is again 8 KV/mm.

High atomic number contaminants greatly increase radiative losses and cool the plasma. Since no sealants are needed, only the quartz walls and platinum alloy electrodes are possible impurity sources. The Soviet experiment shows that this discharge cell minimizes such contamination [1]. Platinum emission lines were never discovered and the quartz molecules sputtered into the plasma radiate significantly only after the maximum temperature, when the pressure is lowered. Air products formed at plasma temperatures are not mentioned, but should similarly emit if present. Thus, the air emission lines under study appear first and are temporarily isolated from the impurity spectra.

CHAPTER III

THE PLASMA FORMATION CIRCUIT

A. Design

The objective of the formation circuit is to produce a pulsed plasma suitable for electrical and spectroscopic analysis--whose complexity depends on the manner of energy deposition. A discharge characterized by a high-current pulse of approximately 50 μs duration is desired to create plasma at any pressure [1]. Quasi-adiabatic energy deposition up to the maximum current can be assumed if the power level and discharge time are properly adjusted to reduce surface losses from the plasma. If the discharge time is long enough to establish thermal equilibrium and to neglect the skin effect and short enough to neglect wall degradation, the quasi-steady-state assumption also applies [4]. Temperature and density gradients become uniformly distributed across the cell. Designing a circuit to produce such a pulse requires AC circuit theory application, construction of devices consequent to this analysis, evaluation of the necessary input energy and corresponding capacitor voltage, and development of high voltage and current monitoring techniques.

The desired pulse can be produced by a slightly underdamped LRC discharge. The basic discharge circuit of

capacitance and total resistance (plasma plus wires) is LRC in nature, with the inductance composed of self-inductance generated by current traversing the magnetic field produced by current in another part of the circuit plus the internal inductance of the capacitor bank. Given the bank, one can adjust the circuit inductance and resistance to obtain the desired discharge time and damping.

The feature point of the LRC circuit is the energy storage mechanisms--the electric field of the capacitor and the magnetic field produced by the inductance. The energy content of the circuit is cycled between them while resistive heating dissipates it into heat. The process is quantitatively described by the following mathematics:

Consider Kirchoff's second law applied to the series LRC circuit shown in Figure III-1:

$$L \frac{di}{dt} + Ri + \frac{q}{C} = 0 \qquad \text{(III-1)}$$

where

L = circuit inductance

R = circuit resistance

C = circuit capacitance

q = instantaneous charge on the capacitor

i = instantaneous current flowing in the circuit

t = time

The three terms represent the respective voltage drops

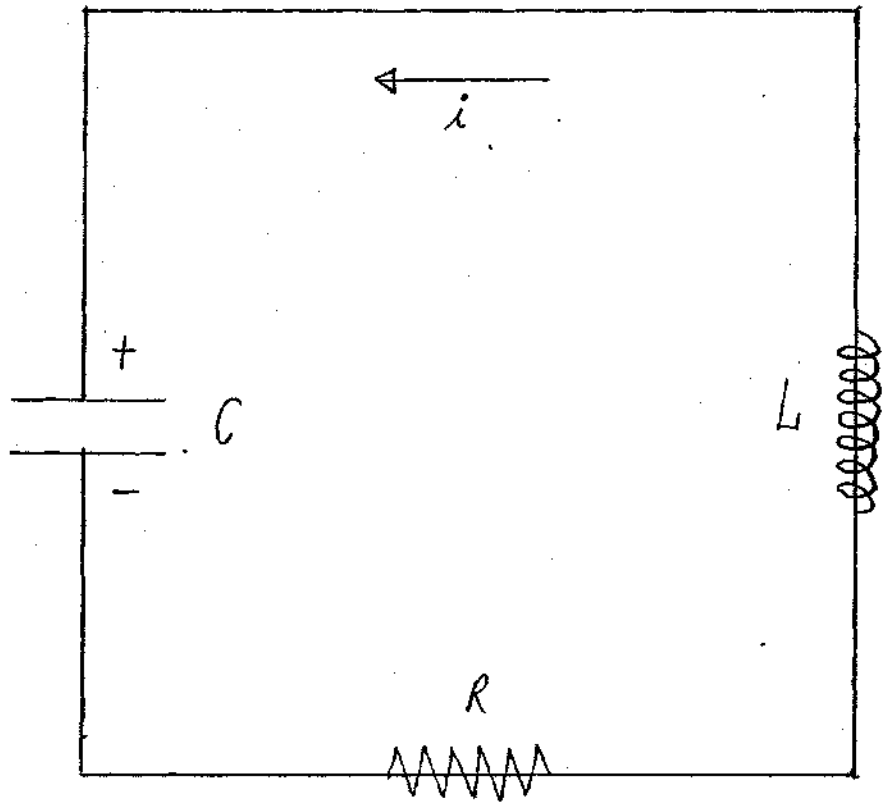

Figure III-1. A Series LRC Circuit

across the inductor, resistor, and capacitor. Since $i = \frac{dq}{dt}$:

$$L \frac{d^2q}{dt^2} + R \frac{dq}{dt} + \frac{q}{C} = 0 \qquad \text{(III-2)}$$

This is the damped harmonic oscillator equation whose solution for constant coefficients is:

$$q = Ae^{-\gamma t} \cos (\omega t - \phi) \qquad \text{(III-3)}$$

where

$$\gamma = R/2L \qquad \text{(III-4)}$$

$$\omega = \sqrt{\frac{1}{LC} - \frac{R^2}{4L^2}} \qquad \text{(III-5)}$$

A, ϕ = constants of integration

The angular frequency ω of the circuit is related to the natural frequency ν by $\nu = \omega/2\pi$ and to the period T by $T = 2\pi/\omega$. An underdamped discharge requires ω to be real and positive.

$$\frac{1}{LC} > \frac{R^2}{4L^2}$$

or

$$L > \frac{R^2 C}{4}$$

The desired waveform is shown in Figure III-2. The oscillation period is 100 μs to satisfy the limitations on discharge time previously discussed, and the initial pulse dissipates 90% of the initial stored energy to satisfy energy deposition requirements and obtain energy economy. This requires heavy damping which attenuates the discharge almost completely after one period. The necessary relative values of two adjacent charge maxima q_i and q_j of the discharge are determined as follows:

$$q_i = Ae^{-\gamma t_i} \cos(\omega t_i - \phi) \qquad \text{(III-6)}$$

$$q_j = Ae^{-\gamma t_j} \cos(\omega t_j - \phi) \qquad \text{(III-7)}$$

where t_i, t_j = time of adjacent charge maxima (current zeroes). Since these times are separated by one-half the period T,

$$t_j = t_i + \frac{\pi}{\omega} \qquad \text{(III-8)}$$

Substituting:

$$q_j = Ae^{-bt_j} \cos(\omega t_i - \phi + \pi)$$

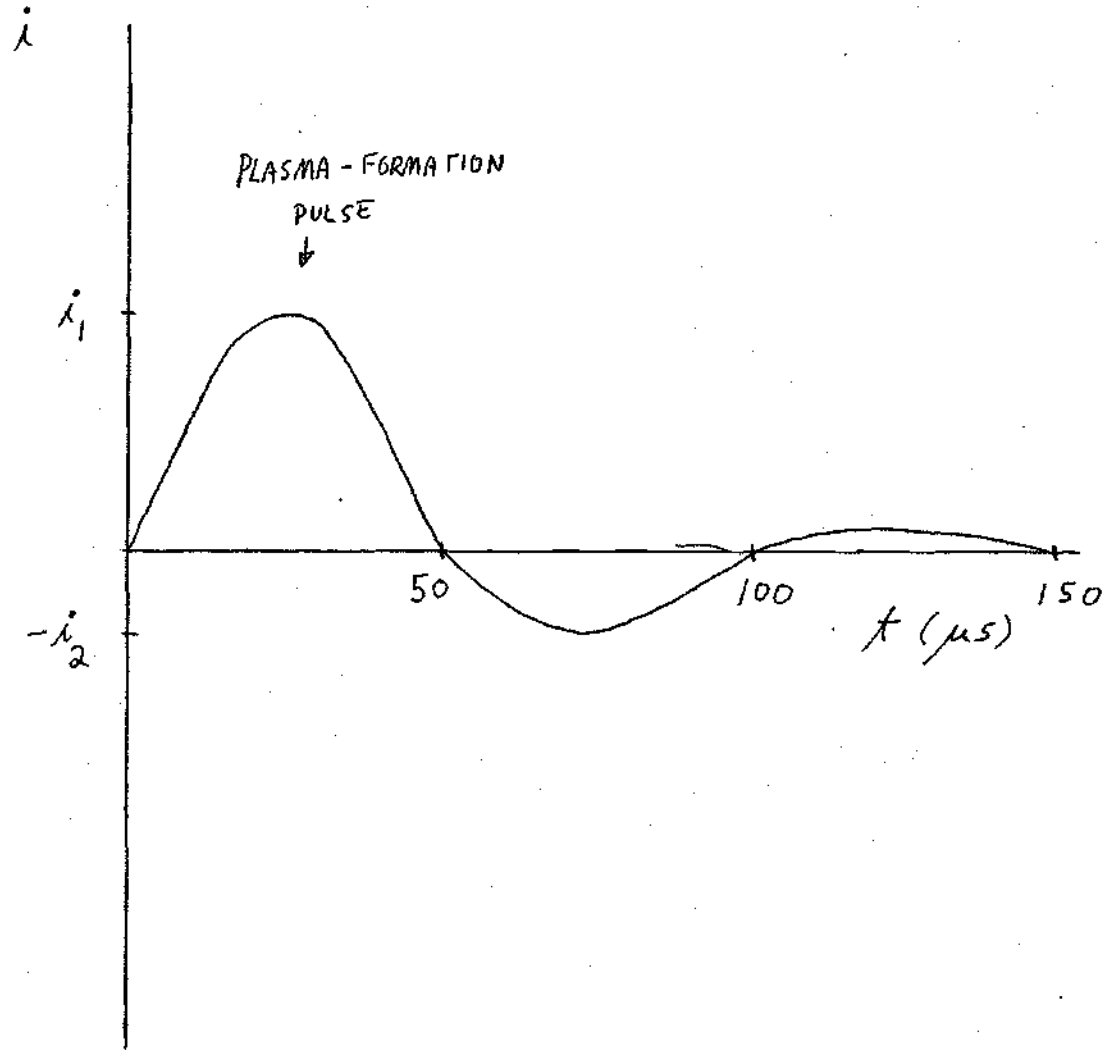

Figure III-2. The Desired LRC Discharge Current

or

$$q_j = -Ae^{-bt_j}\cos(\omega t_i - \phi) \qquad \text{(III-9)}$$

The ratio of equations III-6 and III-9 is:

$$\frac{q_i}{q_j} = -e^{\gamma(t_j - t_i)} = -e^{\frac{\gamma\pi}{\omega}} \qquad \text{(III-10)}$$

At the times of charge maxima, the total energy of the circuit is stored within the capacitor--whose energy E is given by:

$$E = \frac{1}{2}\frac{q^2}{C} \qquad \text{(III-11)}$$

Therefore

$$\frac{E_i}{E_j} = \left(\frac{q_i}{q_j}\right)^2 = e^{\gamma\left(\frac{2\pi}{\omega}\right)} = e^{\gamma T} \qquad \text{(III-12)}$$

The discharge current is determined by differentiation of equation III-3:

$$i = -Ae^{-\gamma t}\left[\gamma\cos(\omega t - \phi) + \omega\sin(\omega t - \phi)\right] \qquad \text{(III-13)}$$

The corresponding peak currents i_k and i_l are:

$$i_k = -Ae^{-\gamma t_k}[\gamma\cos(\omega t_k - \phi) + \omega\sin(\omega t_k - \phi)] \qquad \text{(III-14)}$$

$$i_1 = -Ae^{-\gamma t_1}[\gamma\cos(\omega t_1 - \phi) + \omega\sin(\omega t_1 - \phi)] \qquad \text{(III-15)}$$

where t_k, t_1 = times of adjacent current maxima. Similar to equation III-8:

$$t_1 = \frac{\omega}{\pi} + t_k \qquad \text{(III-16)}$$

Substituting:

$$i_1 = Ae^{-\gamma t_1}[\gamma\cos(\omega t_k - \phi) + \omega\sin(\omega t_k - \phi)] \qquad \text{(III-17)}$$

Thus:

$$\frac{i_k}{i_1} = -e^{\gamma(t_1 - t_k)} \qquad \text{(III-18)}$$

$$\left(\frac{i_k}{i_1}\right)^2 = e^{2\gamma(t_1 - t_k)} = e^{\gamma T} \qquad \text{(III-19)}$$

Comparison of equation III-12 and III-19 show:

$$\frac{i_k}{i_1} = \frac{q_i}{q_j} = \sqrt{\frac{E_i}{E_j}} \qquad \text{(III-20)}$$

Notice that (i,j) and (k,l) can represent any current or charge conditions separated in time by π/ω. If the current ratio $\frac{i_k}{i_1} = 3$, then the ratio of deposition energy of the second and first pulses is:

$$\frac{E_j}{E_i} = \left(\frac{i_1}{i_k}\right)^2 = .111 = 11.1\%$$

Therefore 88.9% of the available energy is dissipated by the first pulse, satisfying the requirements on energy economy heretofore discussed.

The desired current discharge waveform is now specified in both period and damping. Absolute current amplitudes depend on the total energy available--which in turn is set by the plasma pressure desired.

The necessary curcuit inductance and resistance can now be determined for a fixed value of capacitance by examining two characteristics of the LRC discharge:

$$(1) \quad \omega = \frac{2\pi}{T} = \sqrt{\frac{1}{LC} - \frac{R^2}{4L^2}} \qquad \text{(III-5)}$$

Solving for the inductance:

$$L = \frac{T^2}{8\pi^2 C}\left(1 \pm \sqrt{1-\left(\frac{2\pi CR}{T}\right)^2}\right) \qquad \text{(III-21)}$$

$$(2) \quad \left|\frac{i_1}{i_2}\right| = e^{\gamma(t_2-t_1)} \qquad \text{(III-18)}$$

where $|\frac{i_1}{i_2}|$ = magnitude of the ratio of peak currents of the first and second pulse. Since $\gamma = R/2L$ and $t_2 - t_1 = T/2$:

$$|\frac{i_1}{i_2}| = e^{\frac{RT}{4L}} \qquad \text{(III-22)}$$

or

$$L = \frac{RT}{4 \ell n \frac{i_1}{i_2}} \qquad \text{(III-23)}$$

Equating the inductance and solving for the resistance yields:

$$R = \frac{T \ell n \frac{i_1}{i_2}}{C[\pi^2 + (\ell n \frac{i_1}{i_2})^2]} \qquad \text{(III-24)}$$

These solutions are valid for any underdamped discharge. A common approximation based upon $\omega = \sqrt{\frac{1}{LC}}$ instead of equation III-5 is unsatisfactory in this case due to heavy damping.

The required resistance and inductance to create a high-current pulse can now be determined from the following fixed design values:

$C = 3.84\ \mu F$

$T = 100\ \mu s$

$i_1/i_2 = 3.0$

The results are:

$R = 2.58\ \Omega$

$L = 59\ \mu H$

The natural resistance and inductance of the circuit excluding the discharge cell are determined experimentally by replacing the cell with a 2 mm open-air gap with modified electrodes to reduce plasma resistance and discharging the capacitor bank through the gap at the breakdown potential of 1.6 KV. Tungsten cylinders sharpened to points on one end are used as electrodes. The arcover between the points produces a high-current constricted arc before dynamic pressure forces radial expansion whose core conductivity should be greater than that of the cell due to a high initial rate of current rise caused by low circuit inductance. The reduced gap length also reduces plasma resistance at least five-fold. The following information about the circuit was obtained using a Rogovsky coil and oscilloscope for measuring oscillation frequency and damping (this technique is fully explained later in this chapter):

$$T = 12\ \mu s$$

$$i_1/i_2 = 1.2$$

By using equations III-23 and III-24

$$R_E = .06\ \Omega$$

$$L_E = .95\ \mu H$$

where

R_E = resistance of the circuit external to the cell

L_E = inductance of the external circuit

Since the natural inductance of the circuit was measured at about 1 μH, 58 μH must be added via a device called a "choke." A choke suitable for high voltages is essentially a linear air-core solenoid wound with insulated copper wire of a diameter large enough to withstand the large discharge current pulse. The theory of choke design is as follows.

Faraday's law for a long solenoid is

$$\Delta V_s = - \frac{d}{dt} (nl\phi_B) \qquad \text{(III-25)}$$

where

ΔV_s = voltage drop across the solenoid

ϕ_B = magnetic flux produced within the core

n = number of windings in the solenoid per unit length

l = solenoid length

The corresponding voltage drop ΔV_L across an inductor L carrying current i is

$$\Delta V_L = -L \frac{di}{dt} \qquad \text{(III-26)}$$

Since these expressions are equal, integration yields:

$$Li = nl\phi_B \qquad \text{(III-27)}$$

The flux definition and Ampere's law yield:

$$\phi_B = \int_A B \cdot dA = BA \qquad \text{(III-28)}$$

$$\mu_o i_o = \oint B_m \cdot d\ell \qquad \text{(III-29)}$$

or

$$\mu_o(inl) = B_m l \qquad \text{(III-30)}$$

$$B_m = \mu_o in \qquad \text{(III-31)}$$

where

A = cross-sectional area of choke

B_m = magnetic field intensity

i = current flowing through solenoid

i_o = net current passing through the boundary area of the above line integral

ℓ = line integral path

μ_o = permeability constant

The design equation for a choke is then:

$$L = \frac{n l \phi_B}{i} = \frac{\mu_o n^2 l i A}{i} = \mu_o n^2 l A \qquad \text{(III-32)}$$

The inductance is geometrically dependent only and is proportional to its volume (lA) and the square of the winding density. Thus a fat choke with tight windings is desired for minimal length. Actual construction details are presented later.

Having determined the necessary inductance and resistance to produce the desired discharge waveform, the charge and current equations can now be developed as functions of time and initial energy level. The starting point is:

$$q = Ae^{-\gamma t} \cos(\omega t - \phi) \qquad \text{(III-3)}$$

$$i = -Ae^{-\gamma t} [\gamma \cos(\omega t - \phi) + \omega \sin(\omega t - \phi)] \qquad \text{(III-13)}$$

The integration constants are determined by the following initial conditions:

(1) $q = q_o$ at $t = 0$

(2) $i = 0$ at $t = 0$

where

q_o = initial charge on the capacitor.

The results are:

$$\phi = \tan^{-1} \left(\frac{\gamma}{\omega}\right) \qquad \text{(III-33)}$$

$$A = \frac{q_o}{\omega}\sqrt{\gamma^2+\omega^2} = \frac{CV_o}{\omega}\sqrt{\gamma^2+\omega^2} \qquad \text{(III-34)}$$

The current is more conveniently expressed by:

$$i = -Be^{-\gamma t}\cos(\omega t-\theta) \qquad \text{(III-35)}$$

where B,θ = constants of integration

Comparison of equations III-13 and III-35 yields:

$$B = A\sqrt{\gamma^2+\omega^2} = \frac{CV_o}{\omega}(\gamma^2+\omega^2) \qquad \text{(III-36)}$$

$$\theta = \tan^{-1}\left[\frac{\gamma\sin\phi+\omega\cos\phi}{\gamma\cos\phi-\omega\sin\phi}\right] \qquad \text{(III-37)}$$

The following data is used in calculating the above quantities:

$C = 3.84\ \mu F$

$L = 59\ \mu H$

$R = 2.58\ \Omega$

$T = 100\ \mu s$

The constants are then:

$\gamma = 2.19 \times 10^4$ Hz

$\omega = 6.28 \times 10^4$ Hz

$A = 1.06\ q_o$

$B = 7.044 \times 10^4\ q_o$

$\phi = .336$ rad (19.22°)

$\theta = 1.57$ rad (90°)

Using the relation $q_o = CV_o$, the instantaneous charge and current become functions of initial capacitor bank voltage:

$$q = (4.07\times10^{-6})V_o e^{-(2.19\times10^4)t}\cos[(6.28\times10^4)t-.35]$$

$$i = -.270V_o e^{-(2.19\times10^4)t}\cos[(6.28\times10^4)t-1.57] \qquad \text{(III-38)}$$

$$\text{or } i = -.270\ V_o\ e^{-(2.19\times10^4)t}\sin[(6.28\times10^4)t] \qquad \text{(III-39)}$$

where t is expressed in seconds, V_o in volts, and i in amperes, and q in coulombs.

The time of peak current is found by first differentiating equation III-35 to yield:

$$\frac{di}{dt} = De^{-\gamma t}\sin(\omega t-\alpha) \qquad \text{(III-40)}$$

where

$$D = B\sqrt{\gamma^2+\omega^2} = \frac{CV_o}{\omega}\ (\gamma^2+\omega^2)^{3/2} \qquad \text{(III-41)}$$

$$\alpha = \tan^{-1}\ (\frac{\omega}{\gamma}) \qquad \text{(III-42)}$$

The times of peak current t_m are given by:

$$\frac{di}{dt} = 0$$

Therefore

$$t_m = \frac{\alpha+m\pi}{\omega} \qquad \text{(III-43)}$$

where m = 0, 1, 2, 3, ...

The initial and largest current peak corresponds to m = 0:

$$t_{m_1} = \frac{\alpha}{\omega} = 19.7\ \mu s$$

Notice that the current discharge pulse is not symmetric due to the effect of heavy damping. The peak current i_1 of the initial pulse, for which t = 19.7 μs, is given by:

$$i_1 = -.166\ V_o \qquad \text{(III-44)}$$

Power requirements are governed by the amount of energy needed to form a high pressure plasma within the discharge cell. The ensuing design calculations will assume a 100 atm, 10^4°K air plasma as discussed in the preceding chapter. The energy required for its formation equals the sum of the translational, rotational, vibrational, ionization and dissociation energies involved:

$$E_{P\ell} \sim \frac{7}{2} N_D KT + \frac{3}{2} (N_m+N_e) KT + \sum_j \chi_j N_{ij} + \sum_k H_k N_{dk} \quad \text{(III-45)}$$

where:

N_D = number of diatomic molecules in plasma

N_m = number of atoms and monotomic ions in plasma

N_e = number of free electrons in plasma

N_i = number of ions in plasma

N_d = number of molecules which undergo dissociation in plasma

χ = first ionization potential

H = enthalpy of formation

T = temperature of plasma

K = Boltzmann's constant

j = species of ions and molecules

k = species of molecules only

This equation is based upon the following assumptions:

(1) The desired plasma forms during the first quarter cycle of the discharge in a quasi-adiabatic manner. Although radiation does commence synchronously with plasma creation due to the comparatively short relaxation times involved, its quantity is assumed insignificant until the high temperature and pressure of the fully-developed plasma is reached. Further, this formation is assumed to be completed at the time of maximum current (19.7 μs). The remaining energy input combines with high radiative losses to create a

quasi-steady-state plasma for a period immediately following the current peak.

(2) If the plasma is quasi-adiabatic, the temperature of the plasma is uniform until radiative losses cool the peripheral regions and create a non-uniform profile.

(3) Because of the relatively low temperature of 10^4°K multiple or molecular ionization are expected to be insignificant.

Table III-1, based on information from [17], shows which constituents of air are predominant in a 100 atm, 10^4°K plasma. The results are:

$$f_N = .572$$

$$f_O = .238$$

$$f_{N_2} = .1704$$

$$f_T = f_N + f_O + f_{N_2} = .9804$$

where

f_N = mole fraction of dissociated nitrogen

f_O = mole fraction of dissociated oxygen

f_{N_2} = mole fraction of diatomic nitrogen

f_T = total of these mole fractions.

The atoms of nitrogen and oxygen formed by molecular dissociation comprise about 81% of the plasma particle population. Ion population is insignificant in comparison--an expected result since even the first ionization potential of nitrogen and oxygen exceeded the energy associated with the average plasma temperature of 10^4°K. Nitrogen molecules

Table III-1. Constituents of an Air Plasma At 10^4 K and 100 Atm

Species	Mole Fraction
N	.572
O	.238
Ar	.005728
N_2	.1704
O_2	.00023
NO	.00865
N^+	.00134
O^+	.00037
Ar^+	.0000093
N_2^+	.00023
O_2^+	.0000031
NO^+	.00066
e	.00261

Density= .0021 g/cm^3

N= Nitrogen
O= Oxygen
Ar= Argon
e= Electron
+= Ionized

are the only remaining important constituent, comprising 17% of the particles. Only about 2% of the plasma particles are formed by all other processes.

Equation III-45 can thus be simplified:

$$E_{P\ell} \sim \frac{7}{2} N_{N_2} KT + \frac{3}{2} (N_N+N_O) KT + \frac{1}{2} H_N N_N + \frac{1}{2} H_O N_O \qquad \text{(III-46)}$$

where

N_{N_2} = number of nitrogen molecules
N_N = number of nitrogen atoms
N_O = number of oxygen atoms
H_N = enthalpy of formation for nitrogen
H_O = enthalpy of formation for oxygen

The total density ρ of the plasma is .0021 g/cm^3 [17]. The total number of particles N_T is:

$$N_T \sim \frac{\rho V N_{AV}}{f_N M_N + f_O M_O + f_{N_2} M_{N_2}} \qquad \text{(III-47)}$$

where

M_N, M_O, M_{N_2} = molecular weight of N, O, and N_2
V = plasma volume
N_{AV} = Avogodro's number of particles

Input data:

f_N = .572
f_O = .238

f_{N_2} = .1704

M_N = 14 g/g-mole

M_O = 16 g/g-mole

M_{N_2} = 28 g/g-mole

ρ = .0021 g/cm^3

V = 1.1 x 10^{-2} cm^3

N_{AV} = 6.023 x 10^{23} particles/g-mole

The result:

$$N_T \sim 8.39 \times 10^{17} \text{ particles}$$

The ambient particle number N_o is given by

$$N_o = \frac{P_o V N_{AV}}{R_u T_o} \qquad \text{(III-48)}$$

where

P_o = 1 atm = ambient pressure

T_o = 300°K = ambient temperature

Therefore:

$$N_o = 2.69 \times 10^{17} \text{ particles}$$

Thus, particle number increases approximately 3.1 times on transition to plasma mainly by the dissociation process.

Particle numbers for the species involved can now be calculated:

$$N_N = f_N N_T = 4.80 \times 10^{17} \text{ atoms} \qquad \text{(III-49a)}$$

$$N_O = f_O N_T = 2.00 \times 10^{17} \text{ atoms} \qquad \text{(III-49b)}$$

$$N_{N_2} = f_{N_2} N_T = 1.43 \times 10^{17} \text{ molecules} \qquad \text{(III-49c)}$$

The required plasma energy is now found using the following additional data:

$$H_N = 9.76 \text{ eV}$$

$$H_O = 5.06 \text{ eV}$$

$$K = 8.63 \times 10^{-5} \text{ eV/molecule°K}$$

The result on substitution into Equation III-46 is:

$$E_{P\ell} \sim 4.16 \times 10^{18} \text{ eV}$$

$$\sim .67 \text{ J}$$

Of this energy, around 10.4% involved increasing the enthalpy and translational energy of nitrogen molecules, 20.0% involved increasing the translational energy of dissociated atoms, 12.2% was required to dissociate oxygen molecules, and 56.3% went into dissociating the nitrogen molecules.

The capacitor storage voltage required to produce a 100 atm 10^4°K pulsed plasma can be calculated using the quasi-adiabatic energy deposition assumption discussed earlier. Energy is added to the plasma via resistive heating:

$$E_{p\ell} = R_{p\ell} \int_0^{19.7\ \mu s} i^2 dt \qquad \text{(III-50)}$$

where $R_{p\ell}$ is the plasma resistance, which is assumed to be 1 Ω [2]. Since $\theta = \pi/2$, the current given by Equation III-35 can be expressed as:

$$i = -Be^{-\gamma t} \sin\omega t \qquad \text{(III-51)}$$

Therefore:

$$E_{p\ell} = RB^2 \int_0^{19.7\ \mu s} e^{-2\gamma t} \sin^2\omega t\ dt \qquad \text{(III-52)}$$

The solution for the general integral of this kind is [18]:

$$\int e^{ax} \sin^n bx\ dx = \frac{1}{a^2+n^2b^2} [(a \sin bx + nb \cos bx)e^{ax}\sin^{n-1}bx + n(n-1)b^2 \int e^{ax} \sin^{n-2}bx\ dx] \qquad \text{(III-53)}$$

where

$a = -2\gamma$

$x = t$

$n = 2$

$b = \omega$

$\gamma = 2.19 \times 10^4$

$\omega = 6.28 \times 10^4$

$B = .270\ V_o$

Therefore the solution is:

$$\int_0^{19.7\ \mu s} e^{-2\gamma t} \sin^2 \omega t\ dt = 5.88 \times 10^{-6}$$

Equation III-50 becomes on substitution of these values:

$$E_{P\ell} = (4.30 \times 10^{-7})\ V_o^2 \qquad \text{(III-54)}$$

Therefore:

$$V_o \sim 1248\ V$$

This is approximately the capacitor potential needed. Plasma pressure can be determined for a given input energy using spectroscopic analysis. This technique can be employed during actual experiments. It was only necessary to reverse the process for the estimation of required voltage.

C. Monitoring

Monitoring of the high-current electrical discharge requires a system offering protection for both the operator and the low-voltage equipment employed. Two techniques were considered for current monitoring--the current shunt and the Rogovsky coil.

The former is an oscilloscope with a high resistance in series connected across the component under investigation. The resistance experience a large voltage drop which allows measurement of the discharge current with the scope.

The Rogovsky coil shown in Figure III-3, uses the magnetic field generated around wires carrying current to induce a lesser current and electromotance in a surrounding toroidal solenoid. The induced electromotance, which is measured by an oscilloscope, is proportional to the rate of change of discharge current. Current is found by calculation or electronic integration of the signal prior to reaching the scope.

The Rogovsky coil was chosen primarily for safety. When properly insulated, the coil is isolated from the discharge circuit. The shunt is directly connected however, and vulnerable to reflected high voltage pulses generated by the discharge.

The principle of Rogovsky coil operation is as follows: A current is flowing through a wire generates an encircling magnetic field whose intensity B_m diminishes with

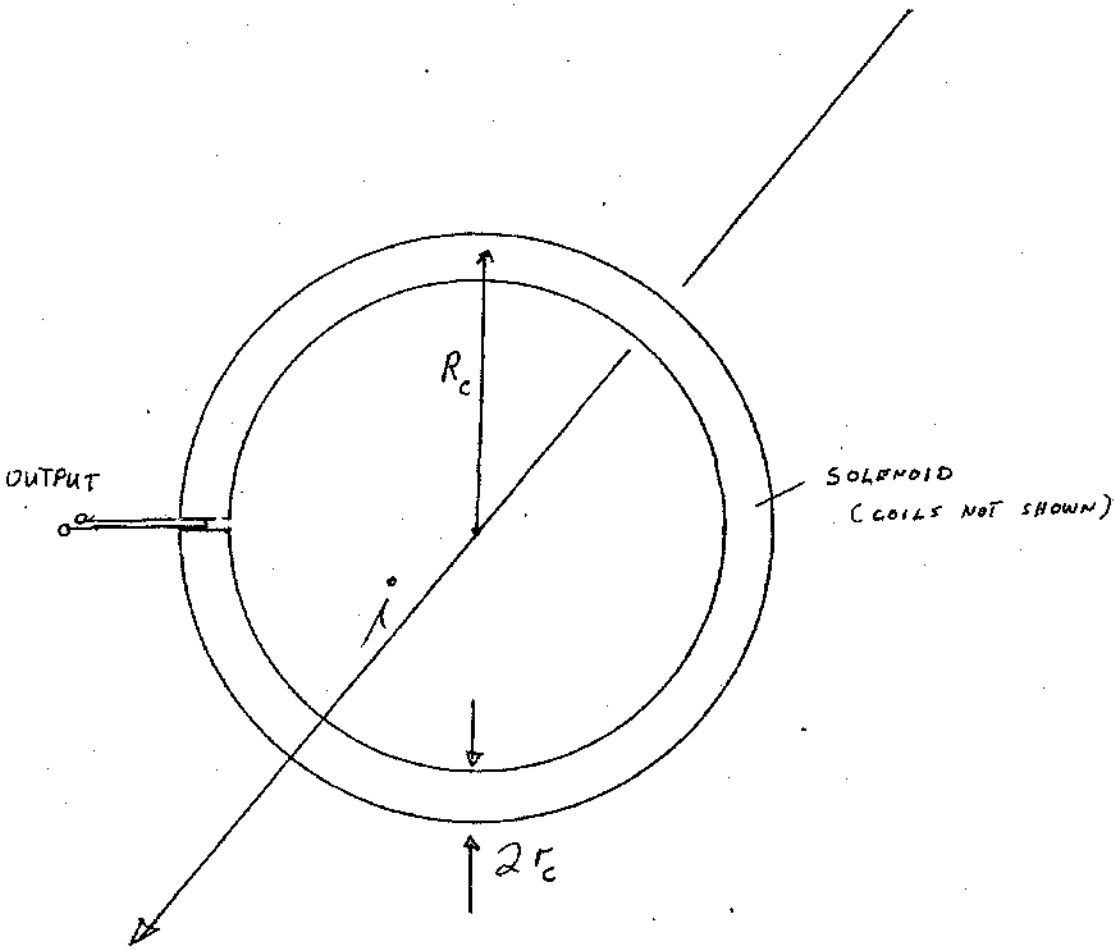

Figure III-3. The Geometry of the Rogovsky Coil

radius in accordance with Ampere's law:

$$\mu_o i = \int B_m \cdot d\ell \qquad \text{(III-29)}$$

Consider a toroidal solenoid surrounding the wire. If its minor radius r_c is much less than its major radius R_c, the magnetic field intensity inside the torus is:

$$B_m \sim \frac{\mu_o i}{2\pi R_c} \qquad \text{(III-55)}$$

The magnetic flux ϕ_B intercepted by the torus is then:

$$\phi_B = \int_A B_m \cdot dA = B_m A = \left(\frac{\mu_o i}{2\pi R_c}\right)(\pi r_c^2) = \frac{\mu_o r_c^2}{2R_c}\, i \qquad \text{(III-56)}$$

where A = cross sectional area of the enclosed portion of the torus. Since the current of a capacitive discharge is time-dependent, the flux is also. A changing flux through a circuit produces an induced current established by an induced electromotive force EMF in accordance with Faraday's law:

$$\text{EMF} = -\frac{d\phi_B}{dt} \qquad \text{(III-57)}$$

For the Rogovsky coil, that law becomes:

$$\text{EMF} = -N\frac{d\phi_B}{dt} \qquad \text{(III-58)}$$

where N = total number of solenoid windings

On substitution for the flux:

$$EMF = \frac{-\mu_o N r_c^2}{2R_c} \frac{di}{dt} \qquad \text{(III-59)}$$

R_c must be small to intercept sufficient magnetic flux within the coil for good coupling. Yet $r_c << R_c$ as previously shown. To achieve an EMF large enough for oscilloscope display, many turns of wire should constitute the solenoid. Consequently, that wire must be of very small diameter d_w. Thus, a general design rule is:

$$d_w << r_c << R_c$$

D. Construction

The design of the discharge circuit based upon the preceding calculations is shown in Figure III-4. Equipment employed is as follows:

(1) 2 1.92 μF 60 KV fast discharge Maxwell capacitors connected in parallel to produce a bank of 3.84 μF

(2) A 75 KV DC, 5 mA Plastic Capacitors power supply

(3) A 118 VAC Variac step-down transformer

(4) A 50 MΩ current limiter composed of 5 10 MΩ 10W "dogbone" resistors in series

(5) A 58 μH inductive choke

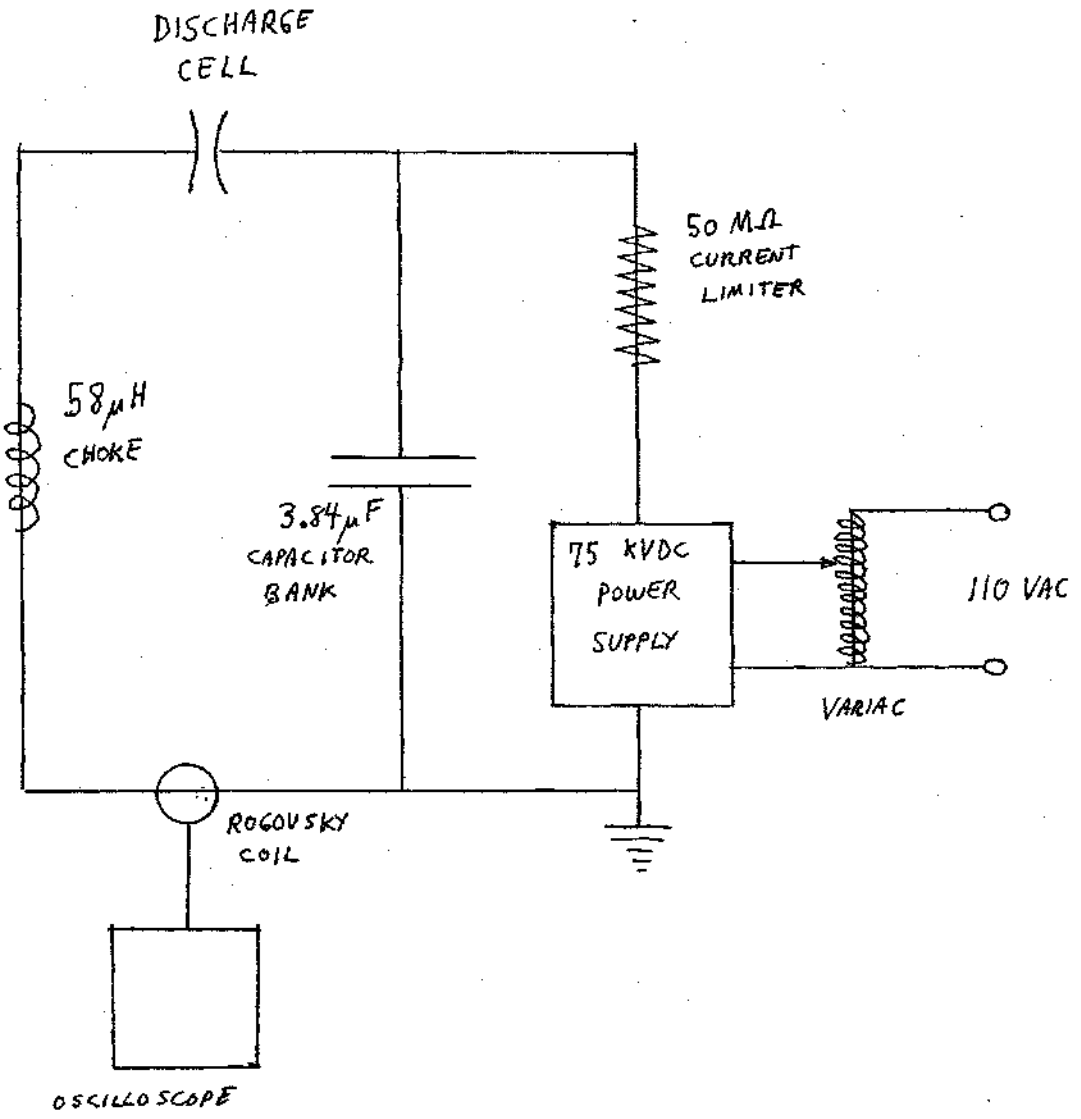

Figure III-4. The Plasma-Formation Circuit

(6) Discharge cell

(7) Rogovsky coil

(8) 555 Tektronix dual-beam oscilloscope

(9) 60 KV R6-8U coaxial cable

(10) General Electric insulated (15 kv) copper wire

The 3.84 μF capacitor bank is charged to the desired potential via the power supply. The latter's voltage output is governed by a fused Variac transformer which feeds its primary windings. A current overdraw from the power supply is prevented up to 50 KV by adding to the charging circuit of the capacitor bank a 50 MΩ current limiter, composed of 5 10 MΩ , 10 W dogbone resistors in series. The required resistance was determined as follows:

Maximum power supply output current i_m = 5 mA

Maximum desired voltage level V_m = 50 KV

Resistance of one dogbone R_D = 10 MΩ

Power rating of one dogbone P_D = 10 w

The power supply output current i such that $i < i_m$ produce Joule heating in the dogbone resistor in accordance with:

$$P = i^2 R_D \qquad \text{(III-50)}$$

where P = power load of resistor

To prevent burn-up: $P \leq P_D$

The total required resistance

$$R_T = V_m/i \qquad \text{(III-61)}$$

Combining these equations yields:

$$R_T \geq V_m \sqrt{\frac{R_D}{P_D}} \qquad \text{(III-62)}$$

$$R_T \geq 50\ M\Omega$$

Thus 5 dogbone resistors in series are needed. The associated current is 1 mA--only one-fifth the maximum allowed current. The capacitor is thus slowly charged--due to limitation of resistors at hand.

Various multi-branched current limiters were considered, but this series combination consumed minimal parts. The stack is interconnected by heavy coats of silver-based paint to ensure good electrical contact without the problems at high voltage.

The discharge branch consists of the capacitor bank, the cell, and the choke. The specifications of the choke are:

(1) Core

Material = hollow cardboard cylinder

Outside diameter d_c = 5.3 cm

Cross-sectional core area A = 22.1 cm^2

(2) Windings

Wire = 16 AWG copper wire with 600 V insulation

Outside diameter = .203 cm

Winding density n = 4.92 turns/cm

Resistance $R_w = 1.38 \times 10^{-4}$ Ω/cm

Since the required inductance L is 58 μH, assuming 1 μH of natural circuit inductance, the choke length for tight windings is:

$$\ell = \frac{L}{\mu_o n^2 A} \qquad \text{(III-32)}$$

$$\ell = 8.6 \text{ cm}$$

Total choke resistance R_{ch} is:

$$R_{ch} = \pi R_w d_c n\ell \qquad \text{(III-63)}$$

$$= .097 \ \Omega$$

Since the total necessary resistance R of the circuit is 2.58 Ω, additional resistance R_{add} is needed in accordance with:

$$R_{add} = R - R_{p\ell} - R_E - R_{ch} \qquad \text{(III-64)}$$

where

$R_{p\ell}$ = plasma resistance ~1.0 Ω

R_E = external circuit resistance ~.06 Ω

Therefore:

$$R_{add} \sim 1.36\ \Omega$$

This amount of resistance is smaller than that offered by conventional resistors designed for high-current discharges. A short length of metal with a suitable conductivity can instead be employed, although its selection has not been presently made. A short length is important to prevent a substantial increase in natural circuit inductance.

Wiring of the components is a combination of coaxial and conventional high-voltage wire to minimize stray inductance, which is proportional to the area enclosed by the circuit. The measured inductance is again 1 μH. The laboratory is designed to accommodate such related pulsed experiments as exploding wires, which require a fast discharge.

The construction of the Rogovsky coil is described along with the oscilloscope in the Chapter V.

No switches are needed because at least 8 KV is necessary for interelectrode arcover, while the capacitor bank stores sufficient energy for plasma formation at about 1.3 KV. Firing must then be externally initiated, as outlined in the next chapter.

CHAPTER IV

PREIONIZATION NETWORK

A. Design

For the interelectrode arcover needed for plasma formation, the potential difference across the gap must equal or exceed the breakdown voltage of 8 KV. The stored energy of the 3.84 μF capacitor bank at this level is 123 J--producing enough electrical power upon discharge to easily shatter the quartz cell. Energy levels around 3.2 J at 1.3 KV storage potential will create plasma at a pressure above 100 atm. Since the electrode separation distance remains constant at 10 mm, a discharge at this lesser potential requires a substantial temporary decrease in the dielectric strength of the air gap. This is accomplished by slightly preionizing the air to increase its conductivity. This conductive bridge between the electrodes can be restricted in cross-section, for the capacitor discharge will quickly expand radially to fill the entire cell volume. Preionization allows a capacitor to discharge at any substantial voltage level.

Three techniques were considered:

(1) A thin metallic wire

(2) An interspaced third electrode

(3) A high voltage, low energy pulse.

The first and second were rejected chiefly because of incongruity with cell design--the wire requires cell disassembly for replacement after each shot while the third electrode lessens cell integrity against leakage and complicates the optical analysis. Both methods also introduce high atomic number impurities into the plasma from the metal and sealants involved.

The pulse is more suitable and is the chosen method of preionization. Its advantages are:

(1) No cell disassembly is required

(2) No appendents to cell design are required, as the pulse is introduced via the existing electrodes

(3) Experiments are repeatable

(4) Contamination is minimal since the air is directly ionized.

The goal of the pulsed technique is to temporarily establish a large potential difference across the electrodes of the discharge cell. As shown in Figure IV-1, the potential of electrode 1 is held constant at the capacitor bank storage level. Electrode 2 can be subjected to a voltage pulse of suitable magnitude and duration to induce an arcover during its presence at the electrode. Since the electrode 1 is maintained at a positive potential before firing, a negative voltage pulse can establish the breakdown potential difference across the gap with a lesser amplitude than its positive

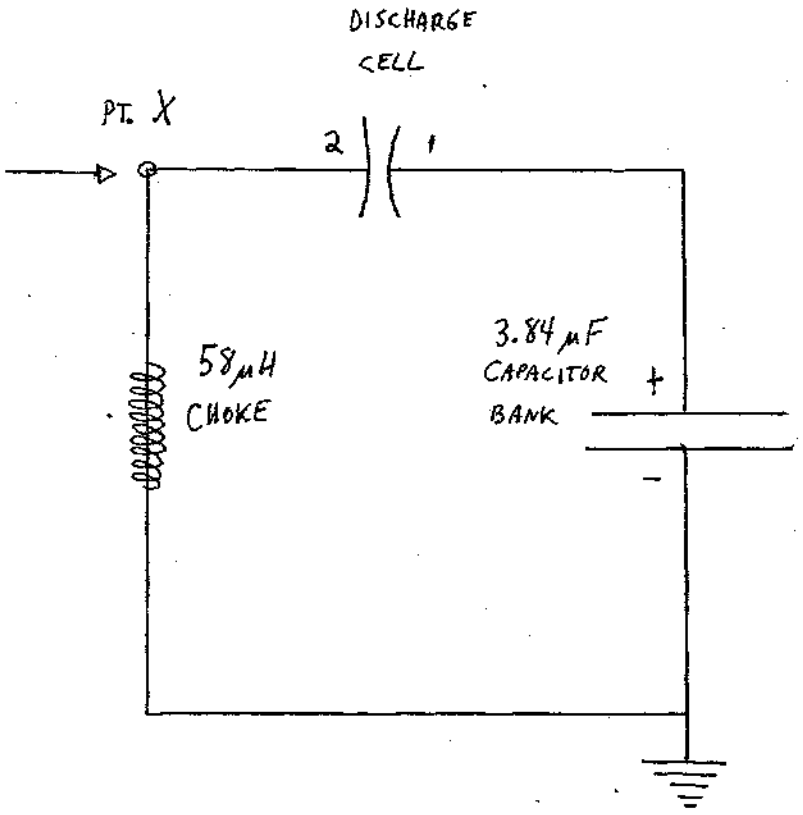

Figure IV-1. Location of Preionization Pulse Entry Into Plasma-Formation Circuit

counterpart:

$$V_{BD} = V_{E1} - V_{E2}$$

$$= V_{E1} + |V_{E2}| \qquad \text{(IV-1)}$$

where

V_{BD} = breakdown voltage

V_{E1} = fixed positive potential of one electrode

V_{E2} = negative potential produced at the other electrode

$|V_{E2}|$ = magnitude of this potential.

Notice that the larger the 3.84 μF capacitor voltage, the less amplitude is required for the pulse.

The optimum location for pulse entry into the discharge circuit must next be determined. It must offer good protection before firing for the network which generates the pulse against a high-current discharge from the charged capacitor bank. The chosen spot is shown in Figure IV-1 as pt. X. Before discharge occurs, pt. X is isolated from high voltage by the cell gap and grounded through the choke.

The pulse must meet several requirements for successful operation:

(1) Its maximum amplitude V_M must establish the breakdown potential across the cell.

$$V_M > 8 \text{ KV} \qquad \text{(IV-2)}$$

(2) Total preionization energy E_p must be small compared to the energy available for plasma-formation E_o to prevent a significant effect on plasma properties. The allowed limit is:

$$\frac{E_p}{E_o} \leq 5\% \qquad \text{(IV-3)}$$

(3) The pulse must continuously maintain a voltage at pt. X of Figure IV-1 at or above the breakdown potential for the length of time Δt necessary for arcover.

$$V \geq V_{BD} \quad \text{for} \quad \Delta t = .4\ \mu s \quad [21] \qquad \text{(IV-4)}$$

Additional desired features for preionization are:

(1) Minimizing the use of high voltage above the laboratory's safety limit of around 12 KV to prevent formation of corona.

$$V_p \leq 12 \text{ KV} \qquad \text{(IV-5)}$$

(2) Pulse formation involves closing a switch in the preionization network presented later. A hydrogen thyratron tube is employed to provide fast, stable high voltage

switching on a nanosecond basis. Its specifications are given in the Appendix. Its jitter time is .005 μs and the pulse should begin to form after this interval to avoid transients.

$$t_F >> .005\ \mu s \qquad \text{(IV-6)}$$

where t_F = time after switch closure that pulse begins to form.

An underdamped LRC discharge can satisfy both mandatory and desired criteria if the proper circuit elements are employed. The proposed preionization scheme is shown in Figure IV-2. Design is accomplished by applying the concepts and formulas developed in Chapter III. Approximations will be used to simplify the analysis, but the system will be designed to be adjustable to allow experimental corrections.

A .001 μF high voltage capacitor is selected for use in the preionization circuit to enable fast discharge at the low energy levels necessary to obey equation IV-3. The circuit inductance and the circuit resistance are each the sum of natural circuit values and that of the components employed. As shown in Chapter III, the stray inductance is about 1 μH and wire resistance is about 1 Ω. The switch, whose identity and characteristics are referenced later, is assumed to be ideal and therefore to contribute neither resistance nor inductance to the circuit. Since the choke

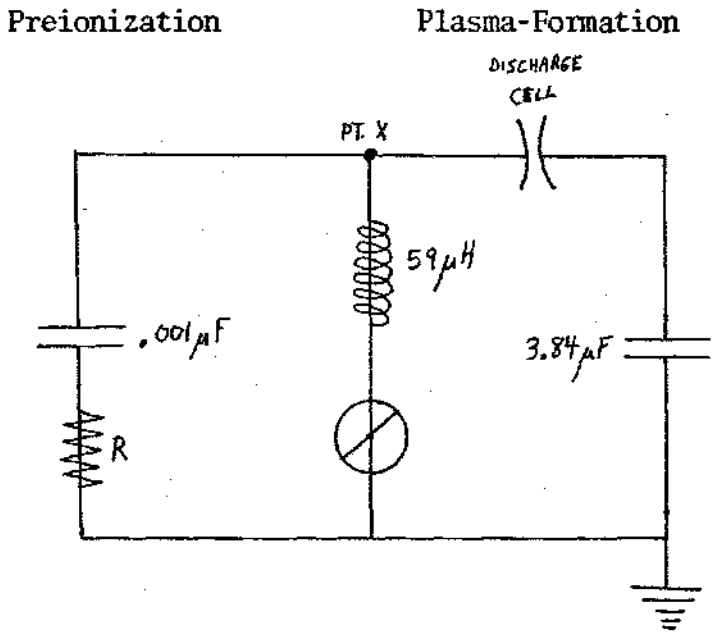

Figure IV-2. Layout of the LRC Preionization Circuit.

inductance is 58 μH and its resistance is about .1 Ω, the total circuit values are:

$$C = .001\ \mu F$$
$$L \sim 59\ \mu H$$
$$R \sim R_A + 1.1\ \Omega$$

where

R_A = the additional resistance shown in Figure IV-2

R = total circuit resistance

As seen by examining Figure IV-2, since the choke is grounded through an ideal switch, the potential at pt. X varies synchronously upon discharge of the preionization capacitor with the negative of the rate of current change in accordance with the equation $V = -L \frac{di}{dt}$. The rate of current change equation is:

$$\frac{di}{dt} = De^{-\gamma t}\sin(\omega t - \alpha) \qquad \text{(III-40)}$$

where

$$D = \frac{CV_p}{\omega} (\gamma^2 + \omega^2)^{3/2} \qquad \text{(III-41)}$$

where V_p = initial storage voltage of the preionization capacitor.

Therefore:

$$V = \frac{-LCV_p}{\omega} (\gamma^2+\omega^2)^{3/2} e^{-\gamma t} \sin(\omega t-\alpha) \qquad \text{(IV-7)}$$

This equation can be significantly simplified by applying the following criteria:

$$V \geq V_{BD} \quad \text{for} \quad \Delta t = .4\ \mu s \qquad \text{(IV-4)}$$

$$V_p \leq 12\ KV \qquad \text{(IV-5)}$$

$$t_F >> .005\ \mu s \qquad \text{(IV-6)}$$

To produce a delayed negative pulse whose peak voltage exceeds the breakdown potential for at least .4 μs but whose initial storage voltage is below 12 KV, small damping is required. The circuit is therefore designed to produce:

$$\gamma^2 << \omega^2 \qquad \text{(IV-8)}$$

where

$$\gamma = R/2L \qquad \text{(III-4)}$$

$$\omega = \sqrt{\frac{1}{LC} - \frac{R^2}{4L^2}} \qquad \text{(III-5)}$$

The minimum circuit resistance of 1.1 Ω is used to minimize damping. Therefore:

$$\gamma = 9.323 \times 10^{3} \text{ Hz}$$

$$\omega = 4.12 \times 10^{6} \text{ Hz}$$

and

$$\gamma^2 = (5.12 \times 10^{-6})\omega^2 \qquad \text{(IV-9)}$$

Since equation IV-8 is satisfied, the following approximations are validated:

$$\omega \sim \sqrt{\frac{1}{LC}} \qquad \text{(IV-10)}$$

$$T \sim 2\pi\sqrt{LC} \qquad \text{(IV-11)}$$

Substitution of data yields the following:

$$T \sim 1.5 \ \mu s$$

$$\alpha = \tan^{-1}\left(\frac{\omega}{\gamma}\right) = 89.9^\circ \sim 90^\circ$$

The voltage equation can thus be simplified:

$$V = -LCV_p\omega^2 e^{-\gamma t}\sin(\omega t - 90°)$$

$$- V_p e^{-\gamma t}\cos\omega t \qquad \text{(IV-12)}$$

A qualitative graph of equation IV-12 is shown in Figure IV-3. The LRC pulse designated for preionizing the discharge cell should be negative in voltage and occur outside the .005 μs jitter region defined by equation IV-6. The chosen pulse is marked in Figure IV-3. Its maximum voltage occurs one-half period after initiation of the preionization discharge. The damping of this pulse is:

$$e^{-\gamma t} = e^{-\frac{\gamma T}{2}} = .99 \qquad \text{(IV-13)}$$

Damping is thus insignificant to design precision. The voltage equation can thus be further simplified:

$$V = V_p\cos\omega t \qquad \text{(IV-14)}$$

The instant of time t_b that the magnitude of the pulse voltage initially equals the breakdown level V_{BD} is given by:

$$V_{BD} = V_p \cos\omega t_b \qquad \text{(IV-15)}$$

$$t_b = \frac{1}{\omega}\cos^{-1}\left(\frac{V_{BD}}{V_p}\right) \qquad \text{(IV-16)}$$

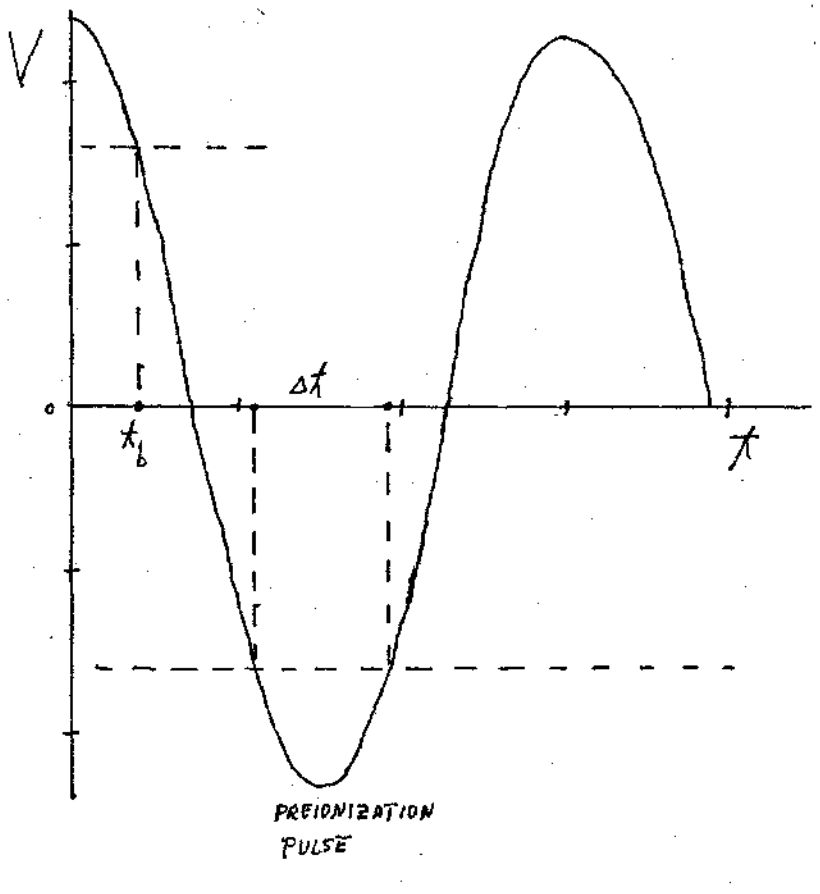

Figure IV-3. Qualitative Graph of Voltage.

Since damping is negligible, the time duration Δt that the voltage magnitude remains above V_{BD} in the pulse of interest is given by:

$$\Delta t \sim 2t_b \qquad \text{(IV-17)}$$

The capacitor is charged to its maximum safe potential of 12 KV. The data is:

$$V_{BD} = 8 \text{ KV}$$

$$\omega \sim 4.12 \times 10^6 \text{ Hz}$$

Therefore

$$t_b \sim .2 \ \mu s$$

and

$$\Delta t \sim .4 \ \mu s$$

The fraction of total plasma input energy is roughly the ratio of the stored energies of preionization and plasma-formation capacitors:

$$\frac{E_p}{E_o} = \frac{\frac{1}{2} C_p V_p^2}{\frac{1}{2} C V^2} = \frac{C_p}{C} \left(\frac{V_p}{V_o}\right)^2 \qquad \text{(IV-18)}$$

where

C_p = .001 μF

C = 3.84 μF

V_p = 12 KV

V_o ~ 1.3 KV

Therefore

$$\frac{E_p}{E_o} \sim 2.22\%$$

The preionization pulse thus meets the design criteria:

(1) The maximum necessary voltage is 12 KV.

(2) The maximum energy of the preionization capacitor is only 2.22% of the plasma-formation capacitor energy before discharge.

(3) The arcover time Δt = .4 μs.

(4) Pulse begins formation $\frac{3}{4}$ T = 1.15 μs after discharge initiation.

B. Construction

The total network designed to preionize the gap is shown in Figure IV-4. The waveform and associated pulse that it produces is shown in Figure IV-5. Components employed in its construction are:

(1) A Plastic Capacitor 50 KVDC, 5 mA power supply, model HV500-502 M.

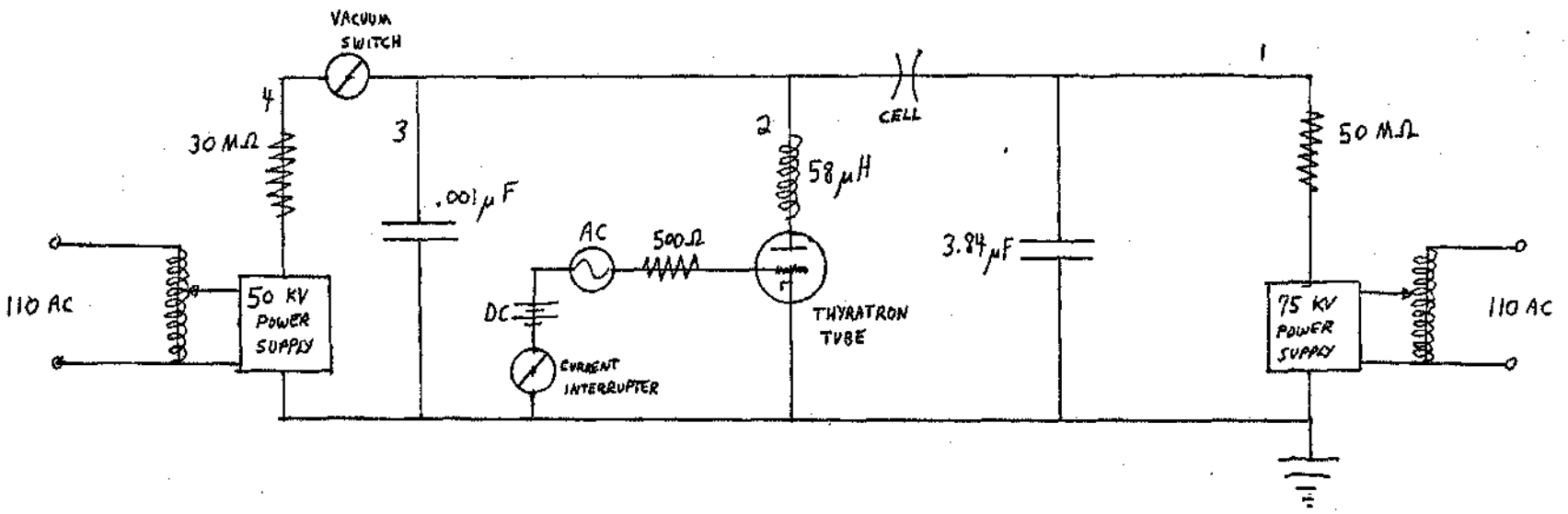

Figure IV-4. The Complete Circuit for Plasma Formation.

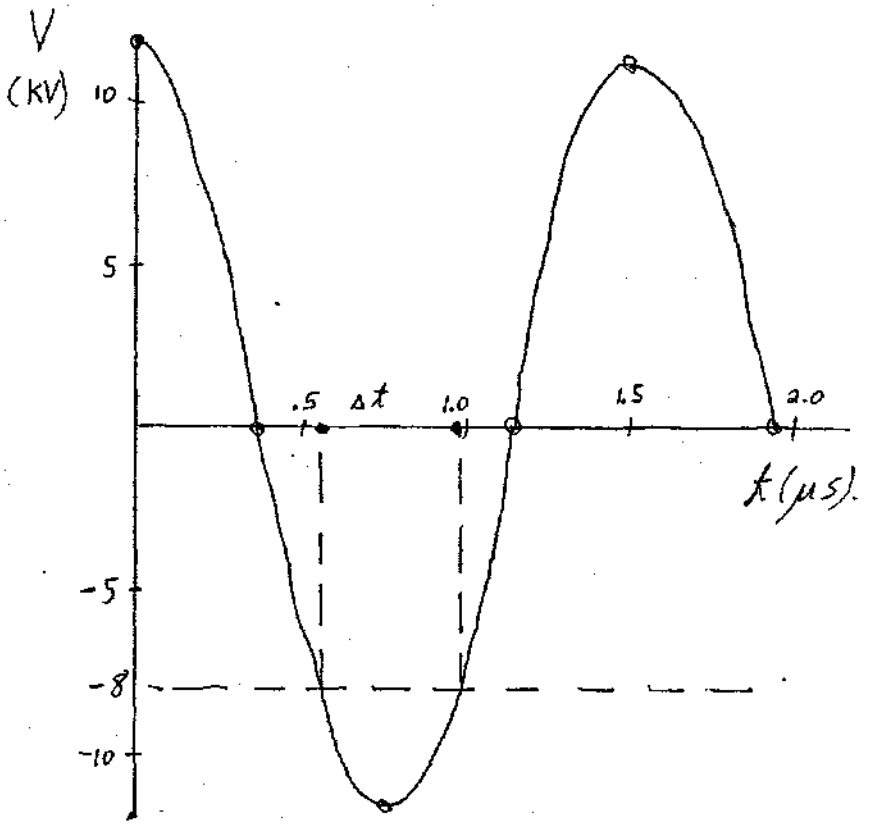

Figure IV-5. Preionization Discharge Voltage.

(2) A Variac step-down AC transformer

(3) Two .001 μF 60 KV Plastic Capacitors, model 600-102.

(4) A Jennings vacuum switch, model RH2G

(5) A Jennings current interrupter

(6) A 5C22 ITT hydrogen thyratron, 325A peak anode current and 16 KV peak forward and reverse anode voltage

(7) Thyratron grid-control equipment:

(a) a variable 1000 VDC power supply

(b) a low voltage high frequency AC power supply

(c) a 500 Ω grid resistor

(8) A 58 μH choke

(9) A 30 MΩ, 10 W current limiter

(10) Insulated (15 KV) General Electric copper wire, type GTO-15.

All components except the thyratron tube were available or produced within the Laboratory or Mechanical Engineering Department.

An unsuccessful experimental attempt at preionization using this set-up was performed using a current interrupter instead of a thyratron, which was then unavailable. Due to its mechanical operation, this switch is unsuitable for microsecond LRC discharges and consumes the majority of the capacitor's energy. Therefore, the preionization waveform probably could not form. The hydrogen thyratron is especially suited for fast capacitive discharges and should

remedy this problem. The thyratron tube should likewise not significantly affect the LRC characteristics of the plasma-formation circuit. The tube inductance and resistance are negligible compared to circuit values.

The hydrogen thyratron tube is essentially a gas-filled triode activated electronically and capable of nanosecond response times for the stable, fast switching not achievable with mechanical switches. The tube's grid has one-way control of conduction, and serves to fire the thyratron at the instant it acquires its critical voltage of 300 V. Once fired, the current is determined solely by external circuit conditions. Thyratron specifications are given in the Appendix.

Supercritical grid voltage is achieved by a barely sub-critical direct grid voltage produced by a variable low current 1000 VDC power supply supplemented by low voltage AC source of suitable frequency as shown in Figure IV-6.* This produces a ripple voltage which exceeds the critical voltage of 200 V during part of its cycle. Resistor R_T = 300 Ω limits the grid current in accordance with the tube's specifications. When the current interrupter is closed, the tube should conduct.

The preionization network offers these additional items:

---

*Details of grid activation will not be presented. The thyratron arrival in the laboratory was subsequent to my departure. Therefore, no familiarization with the device via experimentation was possible. Only the general activation scheme is therefore presented.

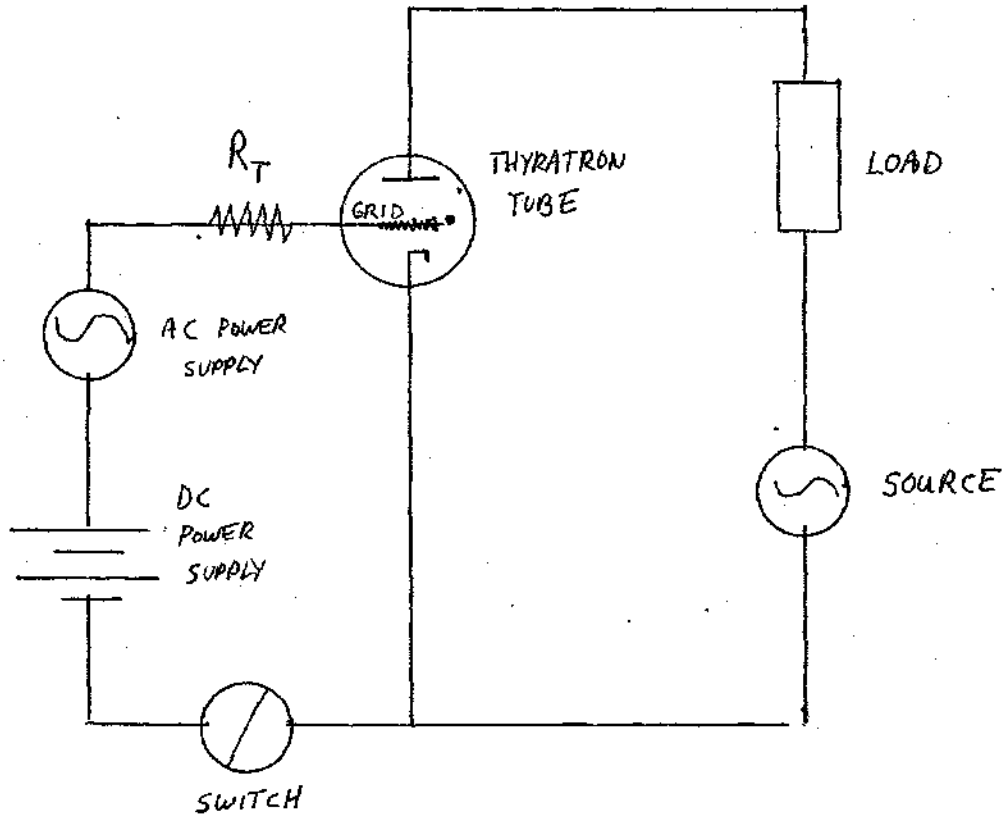

Figure IV-6. The General Thyratron Activation Scheme

(1) Storage potential can be adjusted via a Variac transformer controlling the power supply to any level below the 16 KV limit of the thyratron. Substantial deviations from the design point for experimental corrections are thus accommodated.

(2) Only minimal current leakage from the main circuit during discharge should occur. The impedance of the preionization capacitor is much greater than the impedance offered by the choke, as shown below:

$$Z = R+j(X_C+X_L)$$

$$X_C = 1/\omega C$$

$$X_L = \omega L$$

$$|Z| = \sqrt{R^2 + (X_C+X_L)^2}$$

where

Z = impedance

X_C = capacitive reactance

X_L = inductive reactance

$|Z|$ = impedance magnitude

j = imaginary units

The main discharge at frequency $\omega = 6.28 \times 10^4$ Hz can follow any of the four paths shown in Figure IV-4 to ground. Since

$i = V/Z$, the path of lowest impedance will carry the majority of the current. The impedances of the four routes are:

$$|Z_1| \sim R_{CL1} = 5\times10^7\ \Omega$$

$$|Z_2| \sim \sqrt{R_{P\ell}^2 + (\omega L)^2} = 3.8\ \Omega$$

$$Z_3 \sim \sqrt{R_{P\ell}^2 + \left(\frac{1}{\omega C_P}\right)^2} = 1.6\times10^4\ \Omega$$

$$|Z_4| \sim R_{P\ell} + R_{CL2} = 3\times10^7\ \Omega$$

where

R_{CL1} = 75 KV power supply current limiter resistance (50 MΩ)

R_{CL2} = 50 KV power supply current limiter resistance (30 MΩ)

$R_{P\ell}$ = plasma resistance (1 Ω)

C_P = preionization capacitance (.001 μF)

L = choke inductance (58 μH)

Since $|Z_2| << |Z_1|, |Z_3|, |Z_4|$, the designed main discharge circuit receives the great majority of current as desired.

The system is operated as follows: the .001 μF storage capacitor is charged to 12 KV through a closed vacuum switch and 3 MΩ current limiter by the 50 KVDC power supply controlled by a fused Variac transformer. The power supply is protected against current overdraw up to 30 KV--much

higher than the 16 KV voltage limit imposed by the thyratron. The thyratron is initially open to prevent a premature discharge. The capacitor is isolated from the power supply at the desired voltage level by opening the vacuum switch. The preionization discharge is then initiated by closing the current interrupter switch and thereby activating the thyratron.

CHAPTER V

INSTRUMENTATION AND CONTROL

A. Electrical Data-Gathering Instrumentation

The discharge circuitry is supplemented with the necessary instrumentation to electrically and spectroscopically analyze the plasma and control the high-voltage equipment. Electrical data is assimilated by using the following devices:

(1) The capacitor bank stored energy E_o is determined by measuring its initial voltage V_o in accordance with the following equation:

$$E_o = \frac{1}{2} C V_o^2 \qquad \text{(V-1)}$$

A 100 μA DC meter with an accompanying 150 MΩ series resistance is connected across the terminals of the bank to ascertain its initial voltage via the meter current:

$$\begin{aligned} V_o &= V_A + V_n \\ &= i_n (R_A + R_n) \\ &\sim i_n R_A \end{aligned} \qquad \text{(V-2)}$$

where

R_A = accompanying resistance (ohms)

R_n = internal resistance of the meter (ohms)

i_n = current flowing through meter (amperes)

V_A = voltage drop across resistance (volts)

V_n = voltage drop across the meter (volts)

Therefore,

$$V_o \sim (1.5 \times 10^8) i_n$$

The maximum measurable bank voltage for i_n = 100 μA is:

$$V_{o_{max}} = 15 \text{ KV}$$

The 150 MΩ resistor stock is composed of 10 15 MΩ , 2W resistors in series. The power load of each resistor is:

$$P_a = i_n^2 R_a \qquad \text{(V-3)}$$

where

R_a = resistance of one of the resistors constituting the stock

P_a = power loading of that resistor

The maximum power load is therefore:

$$P_{a_{max}} = .15 \text{ W}$$

The stock should not experience any power overload and subsequent burn-out.

Calibration was also experimentally performed using a 6000 V Triplett meter to directly measure the voltage of the capacitor bank. Five data points were taken--the results showing the linear relationship of meter reading and bank voltage are depicted in Figure V-1. The experimental result agrees with the previous analytical result. Extrapolation to higher potentials is thus validated by Equation V-2.

(2) The rate of change of the discharge current is monitored by the aforementioned Rogovsky coil. The coil is constructed in accordance with design theory results:

$$r_w << r_c << R_c$$

where

r_w = radius of wire used

r_c = minor radius of toroidal solenoid

R_c = major radius of toroidal solenoid

The specifications of this highly-wound coil are as follows:

(1) Wire employed

type--23 gage sheathed transformer wire

diameter--.58 mm

winding density--1.72 1/mm

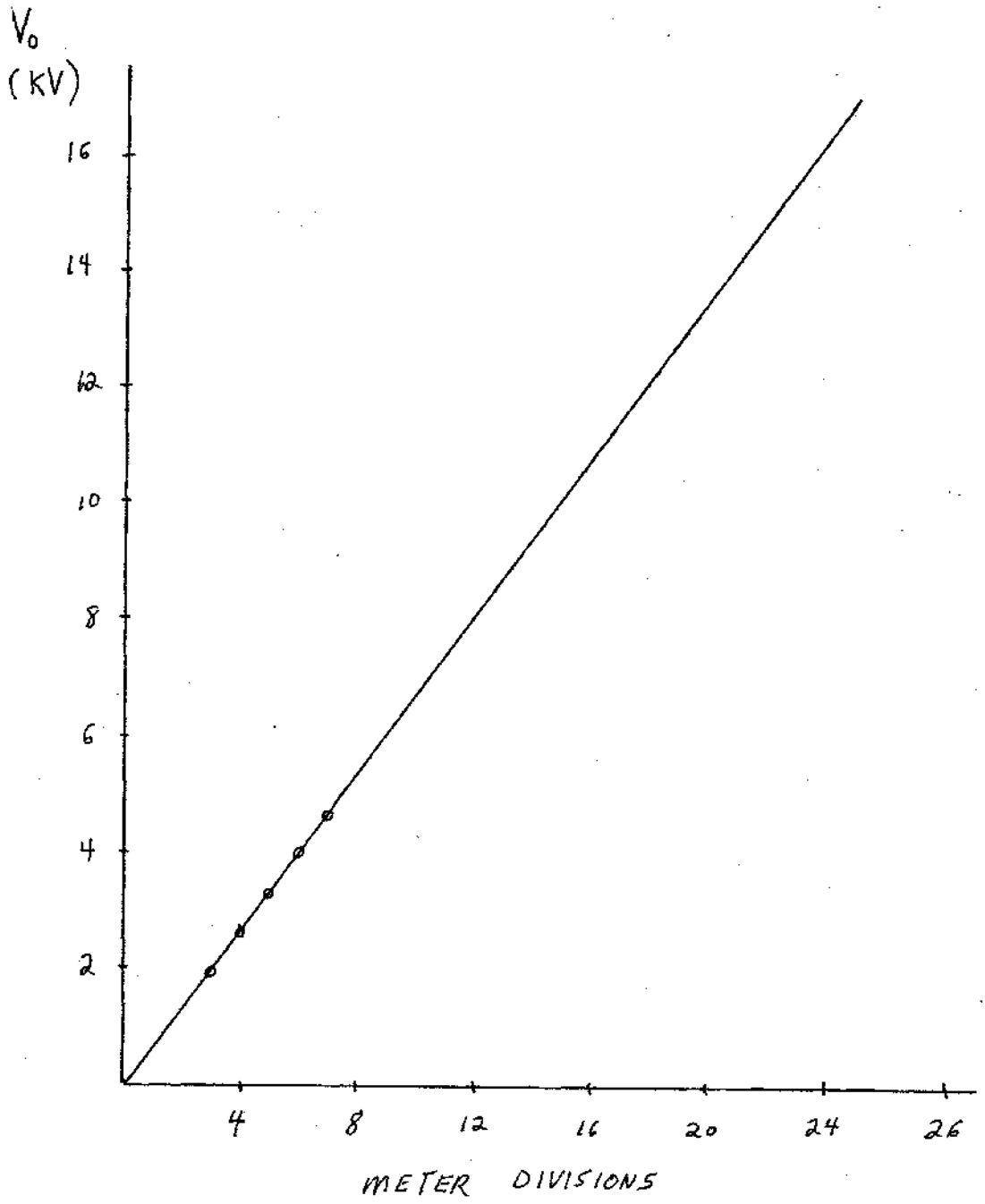

Figure V-1. Capacitor Bank Voltage vs. Meter Reading

(2) Coil

r_c = 2.3 mm

R_c = 16.0 mm

Winding circumference $\ell = 2\pi(R_c - r_c)$ = 86.1 mm

Total windings $N = \ell n$ = 148

The winding base is a coaxial cable of outside diameter $2r_c$ stripped of its outer conductor at the end the coil occupies. The two coil leads are connected respectively to the inner and outer conductors of the cable at each end of the coil. The inner conductor is electrically insulated at this connection by an electrical tape wrapping. The entire coil is likewise covered with electrical tape for safety. In addition, a thick teflon tube is sandwiched between the conductor of the discharge circuit and the Rogovsky coil surrounding it to prevent arcover. The induced electromotance EMF of the Rogovsky coil is related to the rate of change of the discharge current $\frac{di}{dt}$ by:

$$EMF = \frac{-\mu_o N r_c^2}{2R_c} \frac{di}{dt} \qquad \text{(III-59)}$$

By measuring the EMF, current is determined by integration of $\frac{di}{dt}$. Thus, another method of calculating discharge parameters is available and can serve to check the results of the previously described technique. The coupling constant has the following value:

$$\frac{\mu_o N r_c^2}{2R_c} = 3.08 \times 10^{-8}$$

Equation III-59 becomes:

$$EMF = -(3.08 \times 10^{-8}) \frac{di}{dt} \qquad (V\text{-}4)$$

where $\frac{di}{dt}$ is measured in amperes/second and EMF in volts.

Using the expression for current derived in Chapter III, the relationship of initial capacitor voltage to expected EMF peak values can be obtained:

$$i = Be^{-\gamma t} \sin \omega t \qquad (III\text{-}35)$$

The rate of change of current is then:

$$\frac{di}{dt} = De^{-\gamma t} \sin (\omega t - \alpha)$$

where

$$D = B\sqrt{\gamma^2+\omega^2} = \frac{CV_o}{\omega} (\gamma^2+\omega^2)^{3/2}$$

$$\alpha = \tan^{-1} \left(\frac{\omega}{\gamma}\right)$$

Differentiating once again gives the initial points of $\frac{di}{dt}$:

$$\frac{d^2i}{dt^2} = De^{-\gamma t}[-\gamma\sin(\omega t_c-\alpha) + \omega\cos(\omega t_c-\alpha)] = 0$$

where t_c = time of initial peak of di/dt. The result is

$$t_c = \frac{2}{\omega}\tan^{-1}\left(\frac{\omega}{\gamma}\right)$$

The values of the variables are again:

$\omega = 6.28 \times 10^4$ Hz

$\gamma = 2.19 \times 10^4$ Hz

$\alpha = 1.235$ rad.

$c = 3.84$ μF

Therefore:

$$t_c = 39.34\ \mu s$$

$$\left(\frac{di}{dt}\right)_c = (7.184 \times 10^3)V_o$$

where $\left(\frac{di}{dt}\right)_c$ = initial peak value of $\frac{di}{dt}$. Substitution into Equation V-4 yields:

$$EMF = -(2.212 \times 10^{-4})V_o$$

or $$EMF = -.221\ V_o$$

where EMF is measured in volts and V_o in kilovolts. The equation is plotted in Figure V-2.

The coil is connected to a 555 Tektronix dual-beam oscilloscope with mounted time-exposure camera for recording the induced electromotance waveform. The scope's horizontal sweep exhibits non-linearity toward the screen borders and therefore while the upper beam displays the coil waveform, the lower one shows the precision pulses of a multi-marker crystal pulse generator of range 10^{-1} to 10^{4} μs/pulse.

Scope settings are:

Triggering--normal

Vertical deflection--5 V/cm

Horizontal deflection--10 V/cm

Marker setting--10 μs/pulse

Camera and film parameters are:

Shutter speed--time exposure

F-stop--5

Film--Polaroid type 47

Development time--10 sec

Maximum exposure time--approximately 15 sec.

A typical photograph of an underdamped capacitive discharge is shown in Figure V-3. The waveform damping and period reveal via calculation the circuit inductance and effective resistance--hence the current and voltage.

(3) The maximum voltage and energy of the preionizing

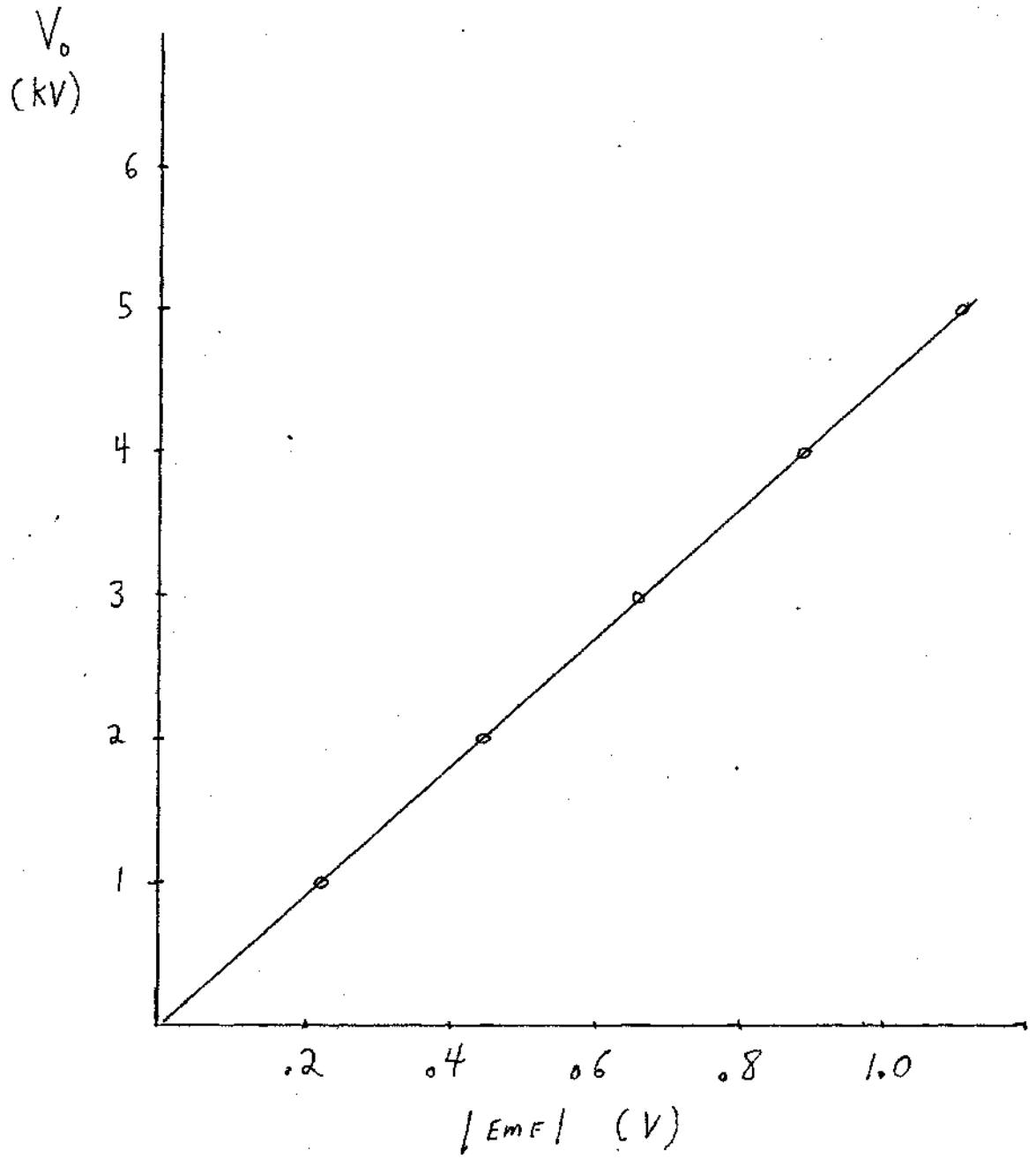

Figure V-2. Capacitor Bank Peak Voltage vs. Rogovsky Coil EMF (Magnitude.)

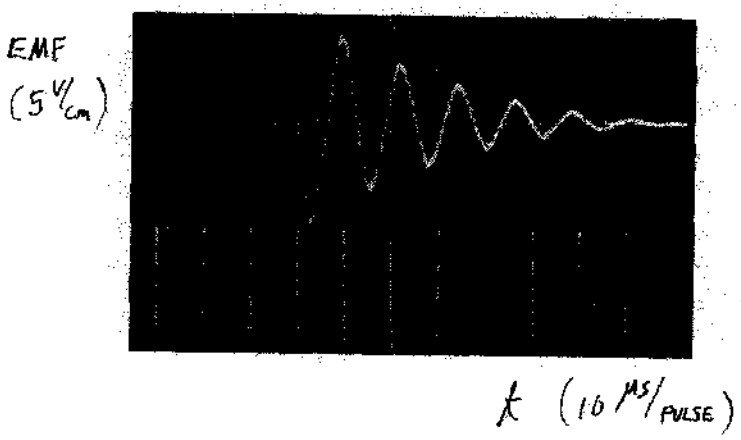

Figure V-3. Rogovsky Coil Measurement of an Underdamped LRC Discharge Using the Pulse Generator

pulse is obtained by measuring the voltage of the 50 KV DC power supply which charges the .001 μF storage capacitor. An AC voltage meter is connected across the primary of this power supply. Calibration using the 6000 V Triplett meter results in the four data points plotted in Figure V-4. Extrapolation to higher potentials is validated as follows, assuming minimal heating of the transformer windings:

$$P_p = P_s$$

$$\frac{V_p^2}{R_p} = \frac{V_s^2}{R_s}$$

$$V_s = V_p \sqrt{\frac{R_s}{R_p}}$$

where:

P_p = power supplied to the primary of the power supply

P_s = power output of the power supply secondary

V_p = voltage drop across primary

V_s = voltage drop across secondary

R_p = resistance of primary winding

R_s = resistance of secondary windings.

The relationship of primary voltage to secondary voltage should thus remain linear.

The 75 KVDC power supply which charges the 3.84 μF capacitor bank is similarly metered across its primary.

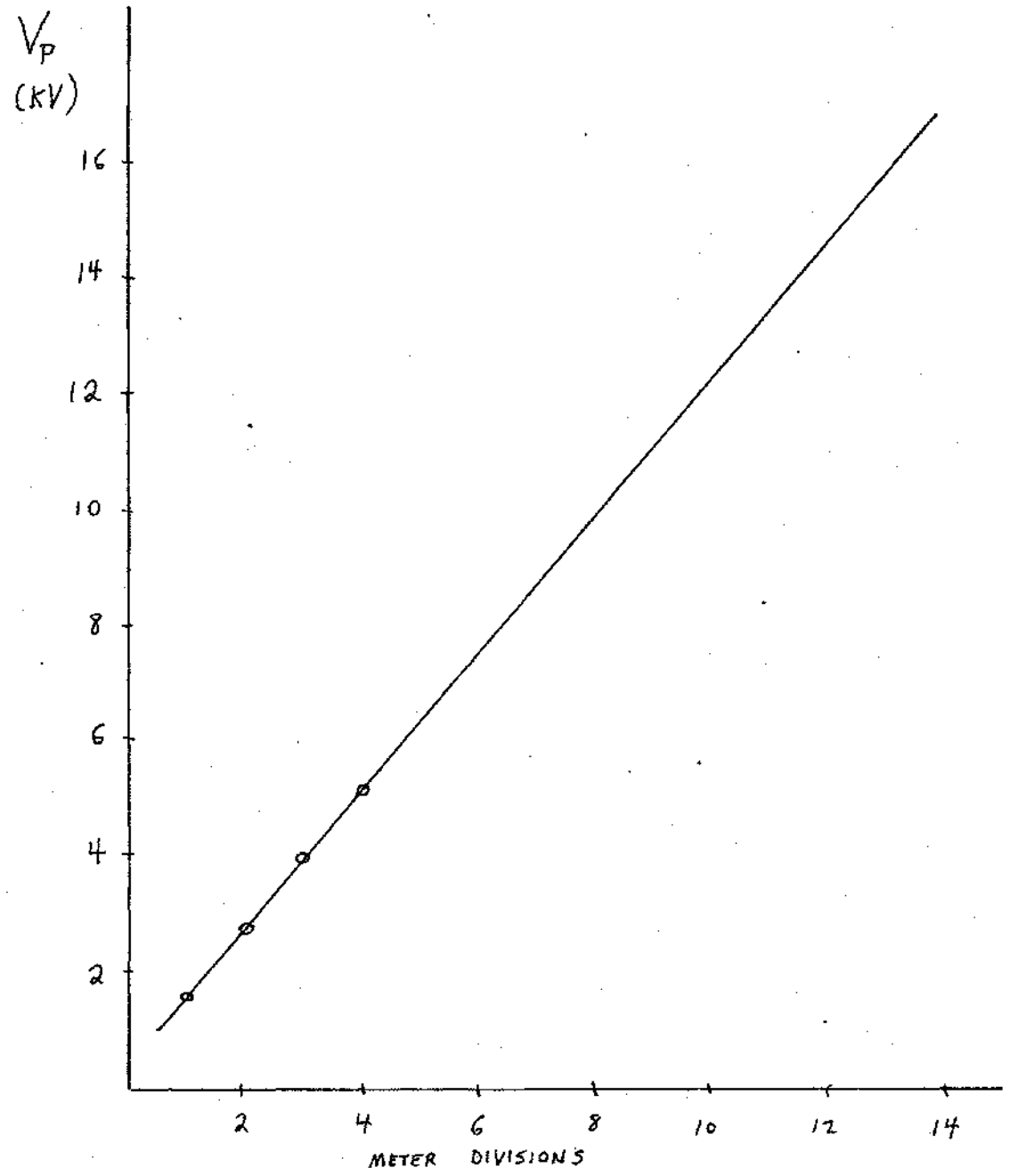

Figure V-4. Preionization Capacitor Voltage V_P vs. Meter Reading

Calibration is superfluous though, since the bank is already monitored. This AC meter is used simply to show whether the power supply has been activated.

B. Spectroscopic Data-Gathering Instrumentation

Radiation emitted from the plasma contains information about such thermophysical properties as plasma temperature, pressure, and electron density. The acquisition and measurement depend upon the plasma state and the diagnostic technique employed. Pulsed plasma analysis is often difficult due to its transient and non-equilibrium nature. As previously discussed however, a pulsed plasma properly created both spacially and temporally can exhibit steady-state behavior during part of its existence and consequently limited thermodynamic equilibrium [4]. The discharge circuit is designed to produce such a plasma via a powerful current pulse and thereby simplify the analysis and calculations.

Conventional spectroscopy is employed to deduce the plasma properties. Probes and microwaves or laser apparatus are considered either incompatible with discharge cell design or insufficiently developed and proven in technique. The objective of the spectrographic instrumentation is the collection of a quantity of radiation within the ultraviolet to near infrared wavelength range from the pulsed plasma sufficient for analysis by a spectrometer. This device separates the various wavelength constituents of the

radiation. Determination of the optimum method for analyzing this information is beyond the scope and purpose of this thesis, but provisions are made for techniques of probable usefulness in designing the apparatus.

The radiation must be transmitted from the discharge cell into the spectrometer. However, the two are located in separate though adjacent rooms. The spectrometer is housed in the Steady-State Laboratory because it offers an air-conditioned climate and greater security than the Pulsed Plasma Facility. Limited floor space for the spectrometer presents a further complication, for its orientation to the plasma source creates a right angle between the direction of radiation emission and the direction required by the entrance slit of the spectrometer.

The optical system designed to overcome these handicaps is shown in Figure V-5. The necessary equipment is:

(1) A Czerny-Turner-type Spex spectrometer employing a reflective grating of 3500 A center wavelength
(2) A 2 m optical bench
(3) 2 fully-adjustable optical stands for supporting the bench
(4) 1 additional stand for supporting a large lens
(5) A convex lens of 16.0 cm focal length and 5.5 cm diameter
(6) A convex lens of 75 cm focal length and 11.5 cm diameter

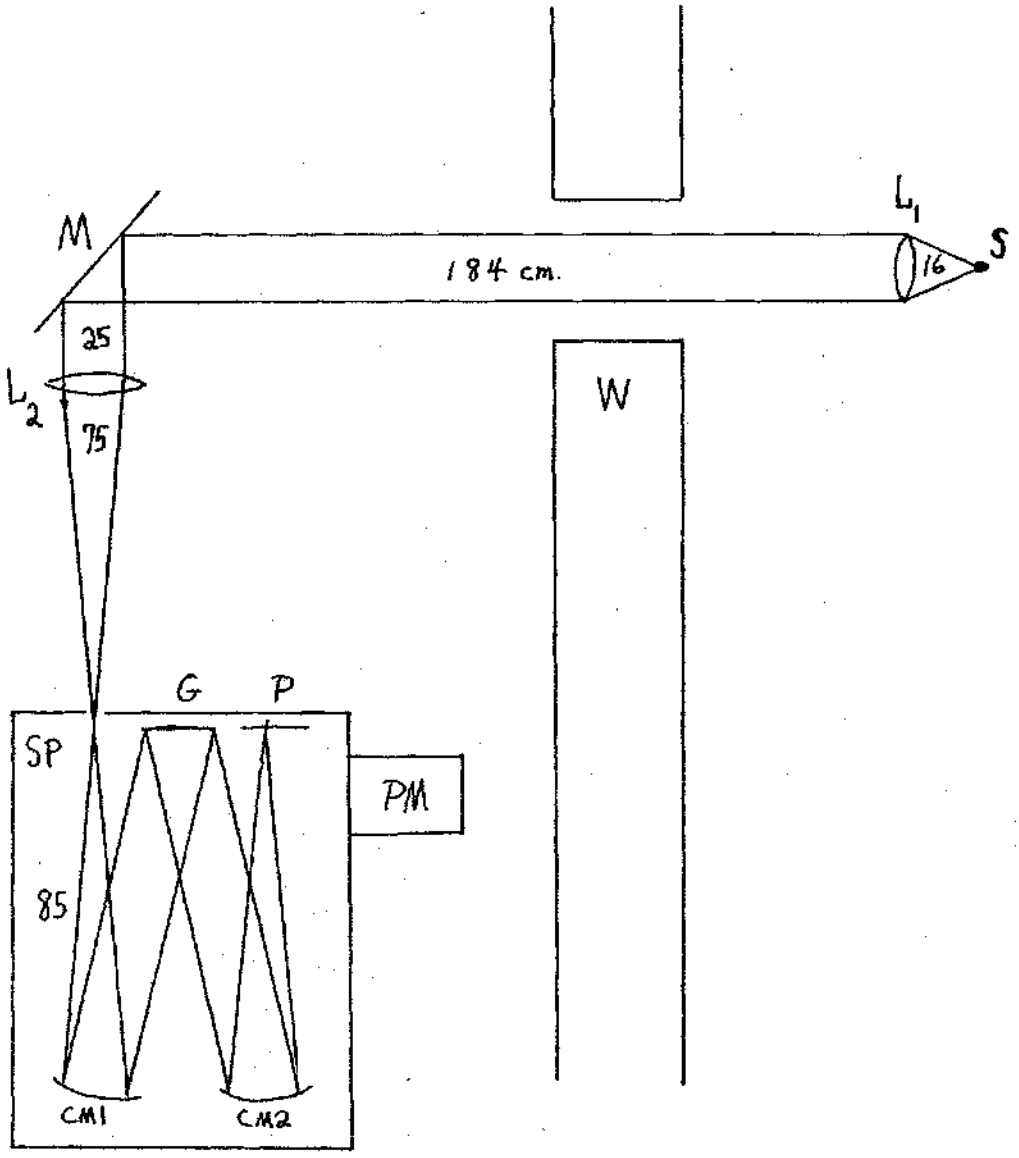

L1 = Lens (f=16 cm)
L2 = Lens (f=75 cm)
M = Plane Mirror
CM1 = Converging Mirror 1
CM2 = Converging Mirror 2
G = Grating

S = Source
SP= Spectrometer
P = Spectrogrphic Plate
PM= Photomultiplier Tube
W = Wall

Figure V-5. Optical System

(7) A 7.62 x 10.2 cm^2 front-surface planar mirror

(8) Assorted clamps and rods for optical mounting

A 40 x 13 cm^2 slot was cut in the dividing wall of the two rooms to provide a 3 m optical path from the source to the spectrometer entrance slit. A stable optical stand was placed on either side of the wall to support a 2 m optical bench spanning the slot. The majority of the optical equipment is located on this bench. The discharge cell can be mounted on the end of the bench using mounting equipment properly insulated. An open-air gap was actually employed during construction and testing. The 5.5 cm diameter converging lense was mounted on the bench at its focal length of 16.0 cm in front of the source. Its close proximity allows interception of approximately 1% of the source radiant energy. Assuming isotropic radiation:

$$\frac{E_L}{E_T} = \frac{\int I \left(\frac{\pi d_L^2}{4}\right) dt}{\int I \left(4\pi r^2\right) dt} = \frac{\frac{\pi d_L^2}{4}}{4\pi r^2} = \frac{d_L^2}{16 r^2}$$

where

E_L = radiant energy intercepted by lens

E_T = total radiant energy

I = intensity of radiation intercepted by lens

d_L = diameter of lens

r = distance from source to lens

Since d_L = 5.5 cm and r = 16.0 cm,

$$E_L/E_T = .74\%$$

In addition, lens theory shows that diverging radiation intercepted by a lens situated at the focal length from the source will continue onward as planar waves:

$$\frac{1}{f} = \frac{1}{0} + \frac{1}{i}$$

where

f = focal length

0 = object distance

i = image distance

If 0 = f, then $i \rightarrow \infty$.

Non-diverging light should thus be transmitted through the slot. A front-surface planar mirror oriented at 45° to the incoming radiation was mounted on the far end of the optical bench to redirected the light towards the spectrometer. A 11.5 cm diameter converging lens which fully intercepted the radiation was mounted on a lens stand and placed at its focal length of 75 cm from the spectrometer entrance slit. An image of the source was formed at the focal point located at the entrance slit and and maximum available signal was thus transmitted inside the spectrometer. The 75 cm focal length is required to insure that the initial converging mirror inside the spectrometer cavity wholly intercepts the diverging radiation passing beyond the entrance slit. The

light is then subject to the Czerny-Turner optics which disunite its components via a reflectron grating centered at 3500 A.

Alignment mechanics in constructing the system were as follows: the source was vertically positioned on the optical bench to match the 115.5 cm mean elevation of the spectrometer entrance slit and laterally adjusted to be directly above the bench. The lens and mirror were similarly aligned. Final adjustments were made by replacing the source with a helium-neon laser. A near-horizontal beam was produced by using a fluid-bubble level placed upon the device. The lens and mirror were then adjusted so that the laser beam pierced each centrally and also intercepted the center of the entrance slit. The open-air source was then replaced and subsequent tests showed that the radiation was indeed focused into the spectrometer slit in accordance with Figure V-5.

Two methods are made available for obtaining useful information from the radiation wavelength separation produced by the spectrometer--photographic plates and the photomultiplier tube. The former shows the relative intensities of line and continuum emissions within a certain wavelength range when irradiated by the spectrum produced by the spectrometer grating. A micro-densitometer can be used to measure the intensity at each wavelength relative to another. 4" x 10" Kodak spectrum analysis plates No. 3 were

selected for use due to their good overall performance as outlined below:

Specifications:

(1) 12.0 relative intensity

(2) Even response over 2500-4800 A range

(3) Medium contrast class

(4) Medium resolving power class

(5) 69-95 lines/mm range

(6) .072 RMS granularity

(7) Medium granularity class

Further details are available in [19]. No spectroscopic plates useful over the entire wavelength range desired were discovered and hence emission intensities at higher wavelength than 4800 A requires another type of plate. A grating centered at a higher wavelength should also be employed.

Measurement of spectral characteristics with a narrow wavelength band is achieved via a photomultiplier tube together with suitable electronics for displaying the output. When connected to the exit slit of the spectrometer, the photomultiplier receives radiation from that portion of the spectrum which intercepts the slit after being redirected by an additional mirror within the spectrometer. The wavelength range depends on slit width, but cannot exceed a few angstroms. Nevertheless, the light produces a photoelectric cascade of electrons within the photomultiplier which multiplies each stage into a measurable current. The magnitude

of the current is directly proportional to the amount of radiant energy received. Conventional picoammeters and pen recorders cannot respond quickly enough to measure the current produced by a radiation pulse of microsecond duration--necessitating the use of high-speed electronic equipment. The laboratory possesses a Tektronix 7844 dual-beam oscilloscope capable of horizontal deflections of 10 ns/cm. It is complemented by a Tektronix C-50 series camera for recording the output on film. This technique can thus measure the relative intensity of an isolated wavelength emission and possibly measure the pulsewidth of a selected line emission.

C. Safety Instrumentation and Control

Operator safety and possible system failure at high voltage received considerable attention. The features of the resulting product are:

(1) An electronic automatic control circuit designed to allow quick deactivation if necessary.

(2) An automatic shorting bar complete with a 10 M 10 Watt dissipation resistor for safe grounding of the capacitor bank at high potentials.

(3) A manual shorting stick for instantaneous grounding of low to moderate voltage components.

(4) An easily identified "panic button" for system shutdown.

(5) An elevated red light which operates when the

system is activated to increase operator awareness of potential danger and warn others entering the laboratory that high voltage is perhaps present.

(6) Fused power supply primaries to prevent current overdraw with subsequent burnout and to guard against reflected high voltage pulses.

(7) Grounding power supplies and capacitor to nearby bus bar.

(8) A high voltage vacuum switch and current interrupter for preionization capacitor charging and thyratron activation. They are connected by a rod of electrically insulative material to a moveable plate electrode.

(9) A wooden shielding wall standing between the control area and the high voltage network to protect the operator against possible explosion.

(10) A lock and appropriate signs on the laboratory door.

(11) Labeled switches to reduce erroneous activations.

The automatic control circuit shown in Figure V-6 operates as follows: Initially, the system is dead--the power supplies are off and the hinged automatic shorting bar rests upon the "hot" terminal of the uncharged capacitor bank. The case being the other terminal is permanently grounded--preventing buildup of stray charge during idle

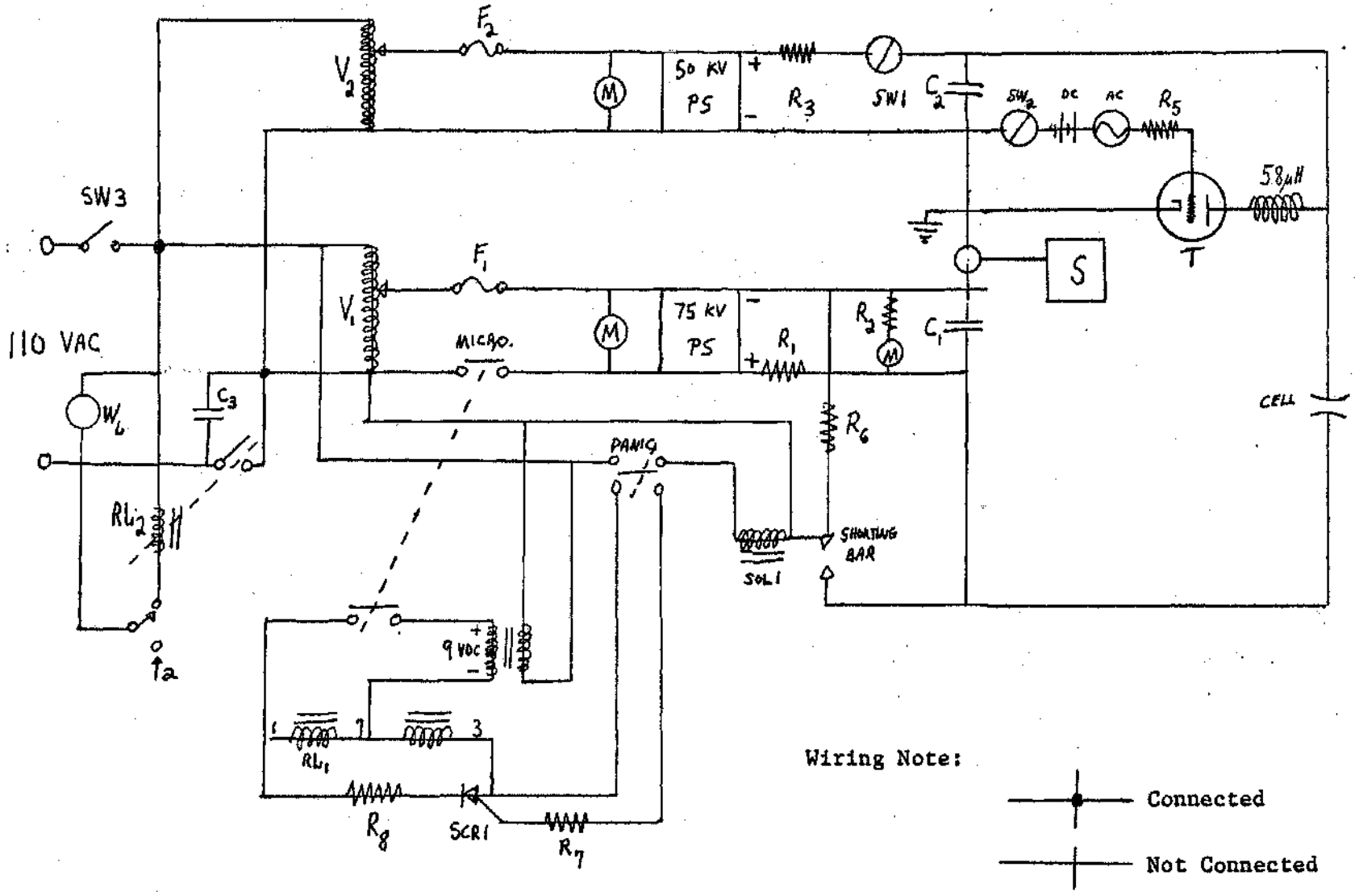

Figure V-6. The Automatic Control Circuit (Legend in Table V-1).

Table V-1. Definition and Values of Symbols Used in Figure V-6

Capacitance:

C_1 = 3.84 μF

C_2 = .001 μF

C_3 = .01 μF

Resistance:

R_1 = 50 MΩ

R_2 = 150 MΩ

R_3 = 30 MΩ

R_4 = 11 Ω

R_5 = 500 Ω

R_6 = 10 MΩ

R_7 = 27 KΩ

R_8 = 12 KΩ

PS = power supply

SW = switch

V = variac transformer

SOL = solenoid

RL = relay

T = thyratron

W_L = red warning light

periods. Activation is a two-step process initiated by closing the fused and lighted main power switch to deliver current to the Variac primaries. The elevated red light is also illuminated and the vacuum switch in the preionization charging circuit becomes operational. The 75 KV power supply remains dead due to the open microswitch-controlled relay in its primary.* Its variac must be turned to zero output to trigger the microswitch and close the relay. A shock-mounted solenoid is also activated which raises and holds the shorting bar several inches above the capacitor terminal. With the system initially at low voltage, charging and experimentation can proceed. Deactivation of the energized power supply and capacitor bank involves simply pressing the "panic button" which triggers the microswitch again to shut off the power--deactivating the power supply and dropping the shorting bar across the terminal of the capacitor bank to slowly discharge its stored energy through the dissipation resistor.

---

*A danger is present resulting from the development of the preionization network subsequent to the automatic control installation. The 50 KV power supply can activate with the main power switch unless its Variac is off--as indicated by its meter. Integration of the power supply into the existing control circuit should preceed further laboratory utilization.

CHAPTER VI

CONCLUSIONS

Several reasons exist for developing the Pulsed Plasma Facility:

(1) It provides a means for creating a 10^4°K plasma at any pressure compatible with the discharge cell structural limitations by simply adjusting the voltage level of the capacitor bank.

(2) Its construction and operation costs are relatively small.

(3) It provides experimental data to support and guide the Steady-State Laboratory.

(4) It avoids numerous problems:

(a) no arc stabilization is required

(b) low power devices can be employed

(c) no wall cooling is needed

(d) chemistry problems are reduced

(e) certain radiative transport problems are lessened

(5) It provides a facility to conduct related experiments--such as exploding wires.

The discharge cell containing the plasma was designed to offer these features:

(1) It is constructed to withstand instantaneous pressures exceeding 100 atm.

(2) It allows numerous discharges without requiring disassembly.

(3) Most parts are easily replaced.

(4) It is electrically protected against arcovers.

(5) Plasma contamination is minimized.

(6) Leakage is minimized.

(7) The quartz walls are 90% transparent to escaping radiation in the wavelength range under study.

(8) It is suited for conventional spectroscopic analysis techniques.

The high pressure plasma is formed by an electrical discharge in a series LRC circuit designed to achieve quasi-adiabatic energy deposition up to the maximum current and quasi-steady-state behavior during a portion of the discharge immediately following. The discharge is slightly underdamped to produce a large current pulse carrying the majority of the initial capacitor energy. The necessary circuit elements are:

$C = 3.84\ \mu F$

$L = 59\ \mu H$

$R = 2.58\ \Omega$

The associated discharge characteristics are:

$T = 100\ \mu s$

$\omega = 6.28 \times 10^4$ Hz

$\gamma = 2.19 \times 10^4$ Hz

Expressions for the instantaneous charge, current, and rate of current change are:

$$q = \frac{CV_o}{\omega} \sqrt{\gamma^2+\omega^2}\, e^{-\gamma t}\cos(\omega t-\phi) \qquad \text{(VI-1)}$$

$$i = \frac{CV_o}{\omega} (\gamma^2+\omega^2)e^{-\gamma t}\sin\omega t \qquad \text{(VI-2)}$$

$$\frac{di}{dt} = \frac{CV_o}{\omega} (\gamma^2+\omega^2)^{3/2}\sin(\omega t-\alpha) \qquad \text{(VI-3)}$$

The governing equations are (graphed in Figure VI-I):

$$q = (4.07\text{x}10^{-3})V_o e^{-.022t}\cos(.063t-.35) \qquad \text{(VI-4)}$$

$$i = -270\ V_o e^{-.022t}\sin(\omega t) \qquad \text{(VI-5)}$$

$$\frac{di}{dt} = (1.8\text{x}10^{7})V_o e^{-.022t}\sin(.063t-1.23) \qquad \text{(VI-6)}$$

The ambient air within the discharge cell requires about .67 J to form a 10^4°K, 100 atm air plasma. 3J of electrical energy stored in the 3.84 μF capacitor bank at an associated potential of 1.25 KV is necessary. The expected peak current during the discharge is:

$$|i_1| = .166\ V_o \qquad \text{(III-44)}$$

$$= 216\ \text{A}$$

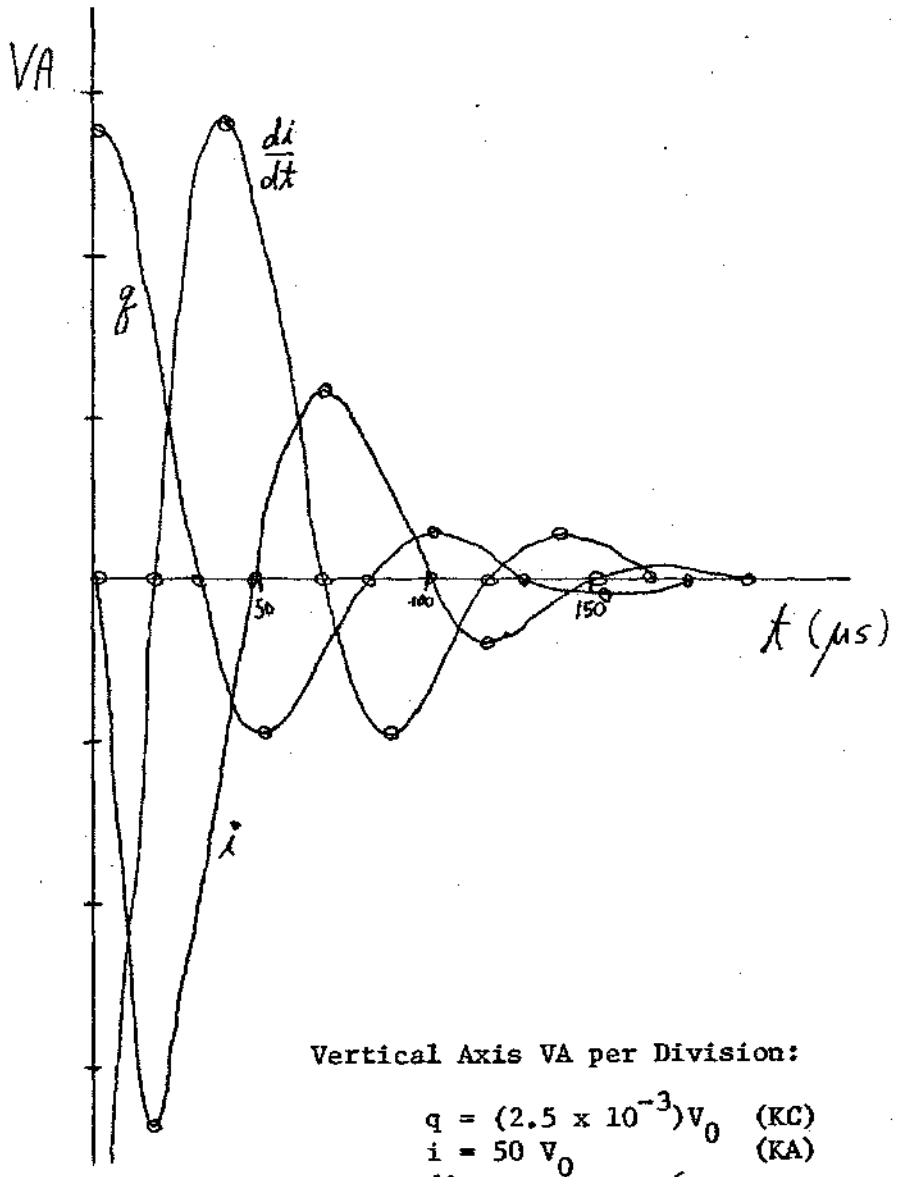

Vertical Axis VA per Division:

$q = (2.5 \times 10^{-3})V_0$ (KC)
$i = 50\ V_0$ (KA)
$\frac{di}{dt} = (2.5 \times 10^{6})V_0$ (KA/sec)

Figure VI-1. q, i, and $\frac{di}{dt}$ of the Main Discharge

The peak power generated by the pulse assuming 1 Ω of plasma resistance is

$$i_1^2 R_{P\ell} \sim 46.7 \text{ KW} \qquad \text{(VI-8)}$$

The preionization technique employed offers the following advantages:

(1) Multi-shot capability.

(2) Capability for discharging plasma-formation energies of variable level.

(3) Capability of varying the power level of the preionization pulse.

(4) Safe preionization voltage levels can be used.

(5) Protection against current leakage from the main discharge.

(6) Minimal discharge energy.

(7) Minimal cell contamination.

Proper values for the elements of the LRC preionization circuit are:

$C = .001\ \mu F$

$L = 59\ \mu H$

$R = 1.1\ \Omega$

The associated discharge characteristics are:

$\omega \sim 4.12 \times 10^6$ Hz

$\gamma \sim 9.32 \times 10^3$ Hz

$T \sim 1.53\ \mu s$

When its capacitor is charged to 12 KV, the preionization circuit produces a negative voltage pulse whose magnitude remains above the 8 KV cell breakdown potential for .4 μs. A study has determined that arcover should occur [21].

Since the peak preionization discharge voltage can be increased to the 16 KV thyratron limit if necessary, the maximum arcover time Δt_{max} according to equation IV-16 is:

$$\Delta t_{max} \sim .51 \ \mu s$$

Instrumentation was devised to measure the plasma's electrical and spectroscopic behavior and to control possible failure modes. The initial voltage level and hence energy level of both capacitor banks are monitored by meters. The electrical discharge parameters L, R, I, di/dt, q, T, ω, and γ are calculated from information available from the Rogovsky coil output. These parameters can be determined via two independent calculational methods. This establishes a check for results. By using a high voltage probe, V and $R_{p\ell}$ can also be determined.

An optical system was designed to guide a portion of the plasma radiation into a spectrometer for analysis. The methods of measurement presently available are:

(1) The relative intensity of emission lines and the continuum within a certain wavelength range can be determined via photographic plates and a densitometer.

(2) Such characteristics of emission lines as line shape and width can be determined using a photomultiplier tube and fast oscilloscope.

(3) Absorption lines can be determined by backlighting the plasma with a reference radiation source. Proper application of these procedures can yield the following thermophysical and transport properties:

(1) Plasma temperature

(2) Plasma pressure

(3) Electron density

(4) Total and spectral emission coefficients

(5) Total and spectral absorption coefficients

(6) Electrical and thermal conductivity.

CHAPTER VII

RECOMMENDATIONS

Although the laboratory has been designed, several constructional details must be completed to make it operational:

(1) The operational requirements of the thyratron must be determined.

(2) The high-voltage probe must be integrated into the main discharge circuit.

(3) The preionization power supply must be incorporated within the automatic control system.

(4) The mounting of the solenoid which holds the shorting bar above the capacitor bank should be improved to reduce noise and vibration.

The following analytical details must be solved in order to gain and interpret useful data:

(1) The quasi-steady-state region of the main discharge current pulse must be defined.

(2) The spectroscopic analysis must be modified to study the plasma radiation emitted during the steady-state phase. Design and addition of a fast-shutter system is suggested.

Long range suggestions involving increasing the capability for spectroscopic analysis are:

(1) Purchase more spectrographic plates which record intensities at higher wavelengths.

(2) Provide an evacuated optical path to allow for vacuum-UV studies.

The final suggestion concerns working conditions. The laboratory needs extensive renovation to provide a professional atmosphere. The following improvements are needed:

(1) A permanent wall to replace the light metal partition presently used.

(2) A tiled floor and suspended ceiling.

(3) Air conditioning.

The laboratory occupies relatively little floor space and these improvements would not be too costly.

APPENDIX

5C22

ELECTRON TUBE DIVISION
P.O. Box 100
Easton, Pennsylvania 18042
Telephone 215 252-7331

HYDROGEN THYRATRON

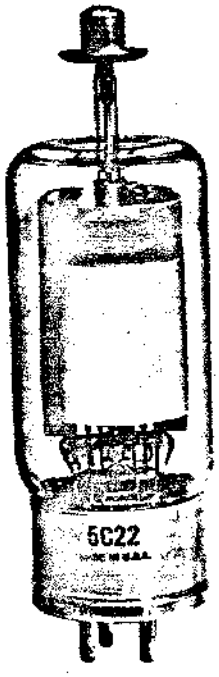

DESCRIPTION

The 5C22 is a unipotential cathode, three element hydrogen filled thyratron designed for network discharge service. In such service, it is suitable for producing pulse outputs of more than 2 megawatts at an average power level of more than 1.6 KW.

The special features of the 5C22 are high peak voltage and current ratings and the compact size, low time jitter and the presence of a reservoir, capable of maintaining the hydrogen pressure throughout the useful life of the tube; an improved and stronger envelope top seal is incorporated.

Electrical Data, General	Nom.	Min.	Max.	
Heater Voltage	6.3	5.9	6.7	Volts AC
Heater Current (At 6.3 Volts)		9.6	11.6	Amperes
Minimum Heating Time		5		Minutes

Mechanical Data, General	
Mounting Position	Any
Base	Super Jumbo 4-Pin with Bayonet A4-18 with Ceramic Insert
Anode Cap	C1-43, Medium, with Corona Shield
Cooling (Note 1)	
Net Weight	12 Ounces
Dimensions	See Outline

Ratings		
Max. Peak Anode Voltage, Forward	16.0	Kilovolts
Max. Peak Anode Voltage, Inverse (Note 2)	16.0	Kilovolts
Min. Anode Supply Voltage	4.5	Kilovolts DC
Max. Peak Anode Current	325	Amperes
Max. Average Anode Current	200	Milliamperes
Max. RMS Anode Current (Note 3)	6.3	Amperes AC
Max. EPY x IB x PRR	3.2×10^9	
Max. Anode Current Rate of Rise	1500	Amperes/ μ Second
Peak Trigger Voltage (Note 4)		
Max. Peak Inverse Trigger Voltage	200	Volts

	Initial Limit	End of Life Limit	
Max. Anode Delay Time (Note 5)	0.65	0.70	Microsecond
Max. Anode Delay Time Drift	0.10	0.10	Microsecond
Max. Time Jitter (Note 6)	0.005	0.01	Microsecond

Ambient Temperature: −50° to +90° Cent.
Shock Rating: 13° Navy (Flyweight) Shock Machine

C22

Two Typical Operations As Pulse Modulator, DC Resonant Charging

Peak Network Voltage	16.0	12.0 Kilovolts
Pulse Repetition Rate	1000	500 Pulses/Sec.
Pulse Length	1.0	1.5 Microseconds
Pulse Forming Network Impedance	47.6	25 Ohms
Trigger Voltage	200	200 Volts
Peak Power Output (Resistive Load 92% Zn)	1.31	1.40 Megawatt
Peak Anode Current	175	250 Amperes
Average Anode Current	0.18	0.19 Amperes DC

NOTE 1: Cooling permitted. However, there shall be no air blast directly on the bulb.

NOTE 2: During the first 25 microseconds after conduction, the peak inverse anode voltage shall not exceed 5 KV.

NOTE 3: The root mean square anode current shall be computed as the square root of the product of peak current and the average current.

NOTE 4: The pulse produced by the driver circuit shall have the following characteristics when viewed at the 5C22 socket with the tube disconnected:

A. Amplitude ..... 200-300 Volts
B. Duration ..... 2 Microseconds (at 70% Points)
C. Rate of Rise ..... 200 Volts/Microsecond (min.)
D. Impedance ..... 50-500 Ohms

The limits of anode time delay and anode time jitter are based on the minimum trigger. Using the highest permissible trigger voltage and lowest trigger source impedance materially reduces these values below the limits specified.

NOTE 5: The time of anode delay is measured between the 26 percent point on the rising portion of the unloaded grid voltage pulse and the point at which evidence of anode conduction first appears on the loaded grid pulse.

NOTE 6: Time jitter is measured at the 50 percent point on the anode current pulse.

Additional information for specific applications can be obtained from the

Electron Tube Applications Section
ITT Electron Tube Division
P.O. Box 100
Easton, Pennsylvania 18042

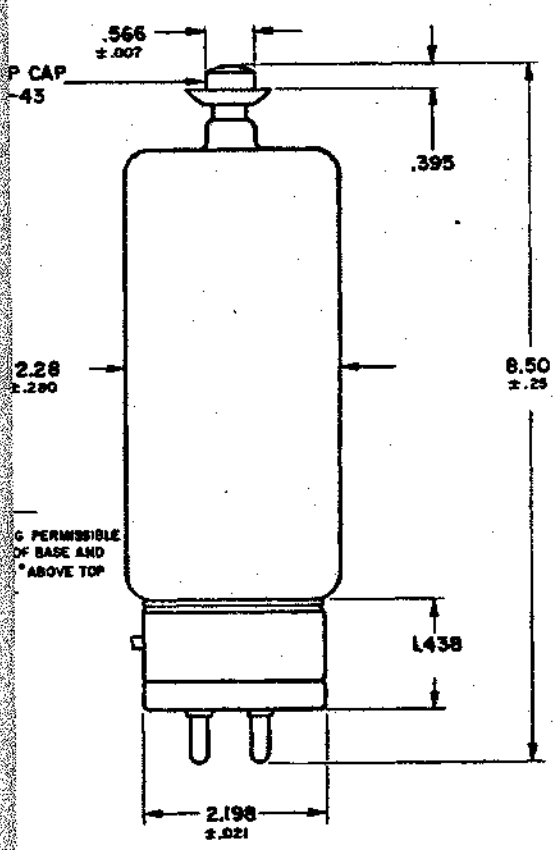

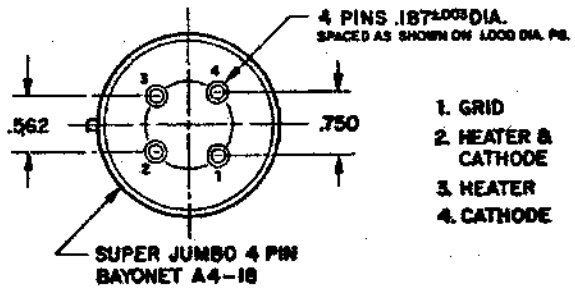

1. GRID
2. HEATER & CATHODE
3. HEATER
4. CATHODE

BIBLIOGRAPHY

1. S. I. Andreev and T. V. Gavrilova, "Investigation of a Pulsed Stabilized Discharge in Air at a Pressure Above 100 atm," translated from Teplofizika Vysokikh Temperatur (High Temperature), Vol. 12, No. 6, pp. 1283-1292, Nov.-Dec., 1974.

2. S. I. Andreev and T. V. Gavrilova, "Measurement of Electrical Conductivity as Air Plasma at Pressures Above 100 atm," translated from TVT, Vol. 13, No. 1, pp. 176-178, Jan.-Feb., 1975.

3. S. I. Andreev and T. V. Gavrilova, "The Thermodynamic Functions of Air at Pressures Above 100 atm," translated from TVT, Vol. 13, No. 4, pp. 868-870, July-Aug., 1975.

4. E. I. Asinovskii and V. A. Zeigarnik, "High-Pressure Discharges," translated from TVT, Vol. 12, No. 6, pp. 1278-1291, Nov.-Dec., 1974.

5. A. A. Bakeev and R. E. Rovinskii, "Electrical Properties of High-Pressure Pulsed-Discharge Plasmas in Inert Gases," translated from TVT, Vol. 8, No. 6, pp. 1121-1127, Nov.-Dec., 1970.

6. G. G. Antonev et al., "High-Current High-Pressure Discharge Chamber I," translated from Zhurnal-Technicheskoi Fiziki (Soviet Physics--Technical Physics), Vol. 42, No. 10, pp. 2121-2126, Oct., 1972.

7. V. I. Petrenko and R. V. Mitin, "Investigation of Internal Structure of High- and Superhigh-Pressure Pulsed Discharges," translated from ZTF, Vol. 45, pp. 1225-1233, June, 1975.

8. F. F. Chen, Introduction to Plasma Physics, Plenum Press, New York, 1974.

9. M. A. Kettani and M. F. Hoyanx, Plasma Engineering, Halstead Press Division, John Wiley and Sons, New York, 1973.

10. W. G. Chace and H. K. Moore, Exploding Wires, Vol. 3-4, Plenum Press, New York, 3rd Edition, 1968.

11. D. Halliday and R. Resnick, Fundamentals of Physics, John Wiley and Sons, New York, 1970.

12. Reference Data for Radio Engineers, Howard W. Sams and Company; Indianapolis, Indiana; 6th edition, 1977.

13. E. R. Peck, Electricity and Magnetism, McGraw Hill, 1953.

14. V. A. Suprynowicz, Introduction to Electronics, Addison-Wesley Publlshing Co., Reading, Mass, 1966.

15. R. R. Huffsey and C. A. Huffsey, Descriptive Electronics, Holt, Rinehart, and Winston, 1970.

16. A. S. Predvoditelev, Physical Gas Dynamics, Pergamon Press, 1961.

17. A. S. Predvoditelev,et al., Tables of Thermodynamic Functions of Air, Infosearch Limited, Cleaver-Hume Press Limited, London, 1958.

18. W. H. Beyer and S. M. Selby, Standard Mathematical Tables, CRC Press, 24th edition, 1974.

19. "Kodak Plates and Films for Science and Industry," Eastman Kodak Company, 1st edition, 1962.

20. "Si-O_2," Heraeus Quartzschmelze, Hanau, 1960.

21. E. O. Lozonskii, "Self-Contained Discharge with a Short Time of Formation at High Pressures," High Temperature, p. 213, March, 1977.